Epithelial micro-invasion by *Streptococcus pneumoniae* induces epithelial-derived innate immunity during colonisation at the human mucosal surface

Caroline M Weight*[1], Cristina Venturini[1], Sherin Pojar[2], Simon P. Jochems[2], Jesús Reiné[2], Elissavet Nikolaou[2], Carla Solórzano[2], Mahdad Noursadeghi[1], Jeremy S Brown[3], Daniela M. Ferreira[2], Robert S Heyderman[1]

[1]Division of Infection and Immunity, University College London, London, United Kingdom, [2]Department of Clinical Sciences, Liverpool School of Tropical Medicine, Liverpool, United Kingdom, [3]Department of Respiratory Medicine, University College London, London, United Kingdom

**Corresponding Author*: Dr Caroline M. Weight, Division of Infection and Immunity, The Rayne Building, 5 University Street, University College London, WC1E 6JF, UK.

Email: c.weight@ucl.ac.uk; Tel: +44 20 3108 2351

ABSTRACT

Control of *Streptococcus pneumoniae* colonisation at human mucosal surfaces is critical to reducing the burden of pneumonia and invasive pneumococcal disease, interrupting transmission, and achieving herd protection. Using an Experimental Human Pneumococcal Carriage Model (EHPC), we show that *S. pneumoniae* colonisation is associated with epithelial surface adherence, micro-colony formation and invasion, without overt disease. Interactions between different strains and the epithelium *in vitro* shaped the host transcriptomic response. Using epithelial modules from a human epithelial cell model that recapitulates our *in vivo* findings, comprising of innate signalling/ regulatory pathways, inflammatory mediators, cellular metabolism and stress response genes, we find that inflammation in the EHPC model is most prominent around the time of bacterial clearance. These results show that rather than being confined to the epithelial surface and the overlying mucus layer, the pneumococcus undergoes micro-invasion of the epithelium that enhances the inflammatory/ innate immune response associated with clearance.

46 **INTRODUCTION**

47

48 Colonisation of upper respiratory tract (URT) mucosa by a range of pathogenic bacteria is a
49 necessary precursor to both disease and onward transmission. Although *Streptococcus pneumoniae*
50 is a common coloniser of the human nasopharynx, it is estimated to be responsible for >500,000
51 deaths due to pneumonia, meningitis and sepsis in children under five years of age worldwide[1].

52

53 In Europe and North America, there has been a dramatic effect of pneumococcal conjugate vaccine
54 (PCV) on vaccine serotype (VT) invasive disease, carriage and transmission[2]. However, the
55 emergence of non-VT pneumococcal disease worldwide and the more modest impact of PCV on
56 colonisation in high transmission settings, threaten this success[3]. Control of pneumococcal URT
57 colonisation in humans is not fully understood[4], and so defining the mechanistic basis for host control
58 of pneumococcal colonisation at the mucosal surface is therefore crucial for the further optimisation
59 of therapeutic interventions which target carriage and transmission. The process of transmission is
60 not fully understood, but mucosal inflammation, potentially enhanced by co-infection with viruses
61 such as Influenza A, has been proposed to mediate bacterial shedding from the nasopharynx[5].

62

63 Naturally acquired immunity to *S. pneumoniae* proteins are primarily mediated by mucosal T cells
64 and anti-protein antibodies, controlled by Treg[6-8]. The role of anti-capsule polysaccharide antibodies
65 in naturally acquired immune control remains unresolved[9]. URT epithelium is central to this
66 immunity[10], binding and transporting antibodies, sensing bacteria via a range of surface and
67 intracellular pathogen-associated molecular patterns (PAMPs) receptors, and rapidly transducing
68 signals to recruit innate and inflammatory immune mechanisms[11,12].

69

70 Murine models suggest that adherence of *S. pneumoniae* to the mucosal epithelium may be followed
71 by paracellular transmigration and tight junction modulation[13,14]. In contrast, studies of immortalised
72 epithelial cell monolayers implicate endocytosis of *S. pneumoniae*, mediated though pneumococcal
73 protein C–polymeric immunoglobulin receptor interactions[15,16]. The relative importance of epithelial
74 endocytosis and paracellular migration in colonisation and invasion remains uncertain[16], but could

influence epithelial sensing of this otherwise extracellular pathogen[14]. For example this may include Nod1 signalling via peptidoglycan[17] and TLR4 signalling via pneumolysin, a pore-forming toxin that induces inflammation and mediates both clearance and transmission in an infant mouse model[18-20].

We have explored the hypothesis that pneumococcal-epithelial engagement dictates the inflammatory/ innate immune response and therefore the outcome of colonisation. Much of what we understand of the control of pneumococcal colonisation is derived from epidemiological studies and murine carriage models. The Experimental Human Pneumococcal Carriage (EHPC) model provides a well-controlled, reproducible tool to characterise the cellular and molecular mechanisms that underlie pneumococcal colonisation in humans[21]. The model has revealed that pneumococcal carriage results in neutrophil degranulation and monocyte recruitment to the nasopharynx[22], protecting against re-challenge with the same strain for up to one year[21,23].

We have used human epithelial cell lines and different strains of *S. pneumoniae* to further probe these mechanisms and derive an epithelial transcriptome module to interrogate the host response in the EHPC model. We show that pneumococcal colonisation in humans is characterised by micro-colony formation, junctional protein association and migration across the epithelial barrier without disease, which we have termed micro-invasion. This pattern of bacterial-host cell association shapes epithelial sensing of *S. pneumoniae,* which is partially pneumolysin dependent. Together, our data suggest that pneumococcal engagement with the epithelium in the early phases of colonisation may occur without eliciting a marked host response, but as colonisation becomes more established, epithelial sensing of *S. pneumoniae* enhances innate immunity/ inflammation which we propose promotes clearance.

101 **RESULTS**

102

103 **Pneumococcal colonisation of the human nasopharynx is associated with epithelial**
104 **adhesion, micro-colony formation and micro-invasion**

105 We have used an EHPC model[21] to capture the epithelial events central to pneumococcal
106 colonisation, obtaining human mucosal samples by curette biopsy. We defined a carrier as an
107 individual colonised by 6B *S. pneumoniae* as detected by culture of nasal wash at any day following
108 inoculation. Clearance was defined as when *S. pneumoniae* colonisation became negative by culture
109 of nasal wash.

110

111 Colonisation was detected in 9/13 healthy volunteers by culture, 12/13 by microscopy (using 6B
112 capsule-specific antibody labelling) and 9/11 by LytA PCR (Table 1). Carriage was detected by
113 culture/ PCR at day 2, whereas maximum detection by microscopy was evident at day 6. This is not
114 explained by colonisation density and therefore the sensitivity of culture/ PCR. This could be
115 explained by greater association with the epithelium (detected by all techniques) rather than the
116 overlying mucus (detected by culture/ PCR but not microscopy) over time. Clearance generally
117 occurred between day 9 and day 27 (Table 1 and Figure 1b).

118

119 Curette biopsy samples visualised by confocal microscopy using Wheat Germ Agglutinin (WGA) as
120 a marker for surface carbohydrates and Junctional Adhesion Molecule A (JAM-A) as a marker of
121 tight junctions, yielded intact sheets of epithelial cells (Supplementary Figure 1bi, 1bii) associated
122 with polymorphonuclear leukocytes, characterised morphologically (Figure 1a and Supplementary
123 Figure 1a). Amongst carriers, pneumococci were found on the epithelial surface (Table 1; Figure 1c,
124 Figure 1d, Supplementary Figure 1biii) which over time (typically by 6 days), consisted of two or
125 more pneumococci at the same location on the epithelial surface, which we have termed micro-
126 colonies (Figure 1e, Supplementary Figure 1biv). There was evidence of what we have termed
127 pneumococcal "micro-invasion" of the epithelial monolayer consisting of either internalisation of
128 bacteria and/ or transmigration across the epithelial barrier (Figure 1e-f). Pneumococci were also
129 observed in phagocytic cells (Supplementary Figure 1a). Colonisation was frequently characterised

130 by co-association between *S. pneumoniae* and JAM-A (Figure 1f). This intimate association between
131 inoculated pneumococci and the mucosa during asymptomatic pneumococcal carriage in humans is
132 suggestive of an active engagement process which may influence the outcome of colonisation.
133
134 Further visualization of this bacteria-host interaction by transmission electron microscopy has proven
135 problematic, but we have been able to demonstrate the integrity of the nasal epithelial curette biopsy
136 samples (Supplementary Figures 1bi and 1bii). We provide evidence of diplococci on the epithelial
137 cell surface and chains or micro-colonies of diplococci that may have been dislodged from the
138 epithelial surface (Supplementary Figures 1biii and 1biv).
139
140 **Epithelial surface marker expression *in vivo* is not altered in response to colonisation with *S.***
141 ***pneumoniae***
142 To determine whether pneumococcal colonisation leads to epithelial activation, we analysed nasal
143 curette biopsy cells for surface expression of molecules expressed in airway epithelium which have
144 previously been shown to be upregulated in response to common bacterial stimuli and are involved
145 in immune cell recruitment. These were EpCAM (for epithelial cell identification), IL-22Ra1, HLADR,
146 CD40, CD54 and CD107a (Supplementary Figure 2a-d). We did not detect a significant change in
147 the relative expression of IL-22Ra1 (protects the epithelial barrier, promotes anti-microbial product
148 secretion during infection, modulating pneumococcal carriage and clearance[24]), HLADR (mediates
149 T cell-antigen recognition and is a marker of epithelial activation[25]), CD40 (co-stimulatory protein
150 which binds CD154[26] (Supplementary Figure 2e-g)), or CD54 (a leukocyte adhesion molecule which
151 is also upregulated by CD40[26,27], initiating neutrophil migration and recruitment[28], Figure 2a).
152 However, although numbers of epithelial cells expressing CD107a did not change over time (Figure
153 2b, left), we observed an increase in CD107a^{high} expression at day 2 post inoculation in carriage
154 positive volunteers vs. carriage negative volunteers (Figure 2b, right). CD107a in the epithelium
155 forms the membrane glycoprotein of late endosomes and phagolysosomes[16] and has previously
156 been implicated in pneumococcal endocytosis[16]. These data highlight the ability of the
157 pneumococcus to colonise the nasopharynx without marked inflammation and potentially implicate
158 CD107a in the process.

159

160 ***S. pneumoniae* infection of nasopharyngeal epithelial cells *in vitro* is associated with**
161 **pneumococcal adhesion, micro-colony formation and micro-invasion**

162 To further understand epithelial responses to *S. pneumoniae* observed in the EHPC model, we
163 undertook infection experiments with Detroit 562 epithelial cells. We compared the 6B response with
164 two other representative clinical isolates; a 23F strain, TIGR4 (the original sequenced strain[29]) and
165 a TIGR4 pneumolysin deletion mutant strain (dPly).

166

167 TIGR4 association with Detroit 562 cells was over 100-fold higher for adhesion and over 70-fold
168 higher for invasion after three hours infection, compared to 6B or 23F strains (Figure 3a-b). Using
169 capsule-specific antibody stain for confocal and electron microscopy, pneumococcal adhesion to the
170 epithelial surface at 3 hours was found to be associated with micro-colony formation, pneumococcal
171 chain formation and internalisation of this conventionally extracellular pathogen[14] (Figure 3d-e,
172 Figure i-j, Supplementary Figure 3a). Internalisation was associated with the formation of epithelial
173 membrane folds (Figure 3j left). Intracellular pneumococci were contained within intracellular
174 vesicles suggestive of endocytosis, which was most marked with the TIGR4 and dPLY-TIGR4 strains
175 (Figure 3b, 3j)[16]. Intracellular pneumococci were seen within vacuoles (Figure 3j middle), coated with
176 JAM-A (a tight junction protein that regulates barrier function and cell polarity, Figure 3f,
177 Supplementary Figure 3a) and associated with the adherens junction protein β catenin (that is
178 involved in epithelial adhesion), but not Claudin 4 (a tight junction protein that regulates paracellular
179 permeability, Supplementary Figure 3a). Pneumococci were located laterally, transiting between cell
180 junctions (Figure 3g, 3j right), at the level of the nuclei and, below the basal membrane (Figure 3h).
181 Transmigration across the epithelium (endocytosis or paracellular movement), as measured by the
182 culture of pneumococci from the basal chamber of transwell inserts, was most marked with 23F
183 (Figure 3c, five-fold higher compared to TIGR4, after three hours infection). A similar pattern of
184 epithelial interaction was also seen at one hour suggesting these observations are not simply
185 explained by differential growth.

186

187 Epithelial infection with the dPly-TIGR4 mutant showed a significant increase in adherence (Figure
188 3a, ten-fold higher after three hours infection), internalisation (Figure 3b, three-fold higher after three
189 hours infection, Figure 3j), but no significant differences in transmigration (Figure 3c) compared to
190 the wild-type strain, implicating pneumolysin in the modulation of bacterial interactions with the
191 epithelium.

192

193 Similar patterns of adherence and invasion were observed in infection experiments with human
194 Calu3 and A549 epithelial cells demonstrating that these findings are cell-line independent
195 (Supplementary Figure 4). Furthermore, primary epithelial cells differentiated on an air-liquid
196 interface for 30 days and co-cultured with either 6B or 23F *S. pneumoniae* also revealed
197 pneumococcal micro-colony formation, micro-invasion and epithelial junctional protein association
198 (Supplementary Figure 1c).

199

200 Together these data show the strain dependency of pneumococcal-epithelial interactions *in vitro*
201 which mirror the epithelial micro-invasion (both internalisation and/ or transmigration of
202 pneumococci) seen *in vivo*.

203

204 **Endocytosis-related micro-invasion and transmigration**

205 To confirm that the pneumococcal endocytosis leads to transmigration across the epithelium,
206 endocytosis was inhibited with dynasore and nystatin[16]. After one hour of infection, cellular uptake
207 of 23F was inhibited by 82% (Figure 4a) and transmigration across the cell monolayer by 85% (Figure
208 4b). This inhibition of endocytosis and transmigration was also seen with TIGR4 (data not shown).
209 In agreement with previous studies using A549 and Calu3 cells[30], we found that viable pneumococci
210 in Detroit 562 cells decreased over time (Supplementary Figure 5a). Using gentamicin treatment to
211 eliminate the original extracellular inoculum, we observed *S. pneumoniae* in the apical and basal
212 media (Supplementary Figure 5b), suggesting egress from the epithelium.

213

214 **Loss of epithelial cell barrier function is not a pre-requisite for micro-invasion by *S.***
215 ***pneumoniae***

216 *S. pneumoniae* has been shown to affect the integrity of epithelial barriers and tight junction function
217 in murine models[13,31]. Having demonstrated pneumococcal micro-invasion without marked epithelial
218 morphological disruption both by confocal and electron microscopy, we explored possible effects on
219 epithelial barrier function by measuring Trans-Epithelial Electrical Resistance (TEER) and
220 permeability to 4kDa FITC-dextran in Detroit 562 cells. TEER was not adversely affected by
221 pneumococcal co-culture (Figure 4c) and permeability was maintained with all the pneumococcal
222 strains at three hours post-infection (Figure 4d). Although co-localisation of pneumococci was seen
223 with host proteins, we did not detect marked epithelial membrane carbohydrate or protein re-
224 distribution (WGA, Claudin 4 JAM-A, β catenin, Supplementary Figure 3a). Similar observations
225 were made with A549 cells and Calu3 cells (Supplementary Figure 4). These data suggest that
226 pneumococcal micro-invasion was not dependent on loss of epithelial cell barrier function during
227 early interactions.

228

229 ***S. pneumoniae* upregulates epithelial surface CD54 and CD107a *in vitro***

230 In a similar manner to primary cells collected from nasal curettes, we assessed Detroit 562 cell
231 surface marker expression in response to *S. pneumoniae* (Supplementary Figure 6a-c). There were
232 no significant changes in IL-22Ra1, HLADR or CD40 expression in response to 6B, 23F, TIGR4 and
233 dPly-TIGR4 strains (Supplementary Figure 6d -f). However, $CD54^{high}$ expression was significantly
234 greater in response to the TIGR4 and dPly-TIGR4 strains, compared to non-infected cells (Figure
235 5a). Epithelial CD107a was upregulated in response to the 6B, 23F and TIGR4 strains (Figure 5b),
236 but this was not seen with dPly-TIGR4. These data implicate pneumolysin in the induction of CD107a
237 but not CD54 epithelial surface expression and support the possibility that CD107a is involved in
238 pneumococcal-epithelial micro-invasion events seen *in vivo*.

239

240 ***Streptococcus pneumoniae* induces epithelial secretion of IL-6, IL-8 and CD54**

241 To assess the inflammatory consequences of pneumococcal-epithelial infections *in vitro*, we
242 measured a cytokine panel in Detroit 562 cell supernatants following *S. pneumoniae* incubation
243 (Figure 5c). We detected a significant increase in IL-6 and IL-8, which were strain dependent and
244 partially pneumolysin dependent. In line with surface marker observations, only TIGR4 significantly
245 upregulated the secretion of soluble CD54, which was dependent on pneumolysin (Figure 5c). These
246 data highlight the less inflammatory nature of the 6B strain compared to the more invasive strain,
247 TIGR4, and the importance of pneumolysin in the epithelial response. Pneumococcal wild-type strain
248 differences were not explained by differences in pneumolysin activity, as determined by hemolysis
249 (Supplementary Figure 7).

250

251 **Innate transcriptomic responses to epithelial infection by *S. pneumoniae in vitro***

252 To explore the hypothesis that the pattern of epithelial adhesion and micro-invasion results in
253 differential epithelial responses, we performed RNAseq of Detroit 562 cells infected with our panel
254 of *S. pneumoniae* strains. In comparison to non-infected epithelial cell cultures, infection with TIGR4
255 upregulated expression of 1127 genes (517 unique genes), 23F upregulated 650 genes (69 unique
256 genes), and 6B upregulated 153 genes (10 unique genes), (Figure 6a). The pneumolysin deficient
257 isogenic mutant of TIGR4 upregulated 220 genes (14 unique genes). Compared to non-infected
258 cells, 1193 genes were upregulated by *S. pneumoniae* infection overall and 93 were core to all
259 strains tested (differentially upregulated genes in Supplementary Excel file 1 and Reactome
260 pathways in Supplementary Excel file 2).

261

262 To elucidate the pathways that drive the transcriptional responses to each strain, we also undertook
263 transcription factor binding site enrichment analysis (Figure 6b, transcription factor binding site
264 enrichment analysis in Supplementary Excel file 3). The responses to 6B and pneumolysin deficient
265 strains were principally enriched in binding sites for the NFkB/Rel family of transcription factors,
266 indicating that an NFkB activation pathway was the dominant driver for responses to these strains.

267 In contrast, cellular responses to TIGR4 and 23F strains revealed enriched binding sites for more
268 diverse transcription factors, suggesting broader molecular pathways by which these strains may
269 influence cellular function. This analysis revealed particular enrichment of binding sites for beta-beta-
270 alpha zinc finger superfamily of transcription factors, including KLF4, suggesting that these strains
271 upregulate mitogen activated protein kinase pathways upstream of these transcription factors[32].

272

273 The sets of genes upregulated by each strain individually were subjected to core and interactome
274 and pathway-enrichment analysis for functional annotation of the cellular response at systems level
275 (Figure 6c). From 20 clusters of pathways, significant enrichment of innate immune system
276 responses was evident in all strains and included specific enrichment in Toll receptor cascades,
277 peptide ligand-binding receptors, NFkB and MAP kinase activation, Interferon signalling and cytokine
278 and chemokine signalling, (Figure 6c, 6d, Supplementary Figure 8). In general, each pneumococcal
279 strain induced a distinct transcriptomic profile, with TIGR4 and 23F strains inducing a broader
280 number of biological pathways than the 6B strain (Figure 6c). Fewer transcriptional responses at the
281 level of functional pathways in response to dPly-TIGR4 is consistent with a role for pneumolysin in
282 innate immune recognition of *S. pneumoniae*[33]. Fewer transcriptional responses to 6B is consistent
283 with our observations that this strain exhibits the lowest level of cellular association and
284 transmigration.

285

286 **Epithelial transcriptomic responses to 6B are detectable *in vivo***

287 Next, we sought to test whether these epithelial transcriptomic responses to *S. pneumoniae* were
288 also evident in the 6B EHPC model. We compared nasal transcriptomes sampled at two or nine days
289 after inoculation to pre-inoculation samples. These revealed enrichment of 162 transcripts among
290 individuals who became colonised (differential gene expression in Supplementary Excel file 4).
291 These genes included Claudin 5 and Claudin 17, Defensin β 103A/B, Cadherin 16, Desmocollin 1
292 and Gap junction protein α1, which suggests cytoskeletal re-organisation two days post-inoculation
293 in carriage positive individuals. By day 9 post-inoculation, molecules such as CCR3, matrix

294 metalloproteinase 12 and MHC II molecules were enriched, suggesting activation of the nasal
295 mucosa[34]. However, these genes were not significantly enriched for any immune response pathway
296 annotation perhaps because of the statistical stringency necessary for genome-wide multiple testing
297 and were not epithelial-specific.

298

299 Gene expression modules can successfully detect specific transcriptional programs in bulk tissue[35].
300 Therefore, as an alternative approach, we sought to target specific epithelial responses *in vivo* using
301 the *in vitro* interactome. A direct comparison of transcripts for 6B revealed FOSL-1, an AP-1
302 transcription factor subunit, to be enriched with carriage, which has previously been reported to
303 become activated following pneumococcal challenge in BEAS-2B and HEK293 cells[36]. To expand
304 the sensitivity of the approach, we evaluated the expression of two transcriptional modules in the
305 nasal samples (Figure 7). A 'core' module comprised of 16 interacting genes (Figure 7b) that were
306 upregulated in the Detroit epithelium by all the pneumococcal strains from Figure 7a, and a second
307 'integrated' module that comprised of 200 interacting genes (Figure 7c), which were upregulated in
308 the Detroit epithelium by at least one of the pneumococcal strains from Figure 7a. Among carriage
309 negative individuals, we found no increase in expression in either gene expression modules (Figure
310 7b-c). In contrast among the individuals who became colonised, the increased expression of both
311 modules, (significantly increased within the integrated module, Figure 7b,7c), suggests that the
312 prominence of responses at day nine may reflect time-dependent proliferation of the 6B bacterial
313 inoculum, epithelial engagement and the subsequent epithelial activation. These responses coincide
314 around the time of bacterial clearance.

315

316

317 **DISCUSSION**

318 It is widely accepted that colonisation of the URT mucosa by many potentially pathogenic bacterial
319 species, involves transient association with the overlying mucus layer but that adherence to the
320 epithelial surface avoids mucus entrapment and muco-ciliary clearance[14,37]. While evading immunity,

321 bacterial replication then occurs prior to onward transmission to a new host. Even for *S. pneumoniae,*
322 the mechanisms underlying this transition from acquisition to established colonisation, and then
323 transmission and/or disease, are not well understood. By combining an EHPC model and *in vitro*
324 human cell culture systems, we show that pneumococcal colonisation leads to epithelial adherence,
325 micro-colony formation and migration across the epithelial barrier without disease, which we have
326 termed micro-invasion. The finding of co-association with junctional proteins provides a possible
327 mechanism for micro-invasion. Clearance of the pneumococcus from the mucosa *in vivo* occurs in
328 the context of micro-invasion. Indeed, epithelial micro-invasion and not bacterial load *per s*e, appears
329 to dictate unique transcription factor binding site signatures, downstream cytokine, chemokine and
330 metabolic pathway enrichment (Figure 8).

331

332 The concept of mucosal micro-invasion moves us away from current models of colonisation where
333 the pneumococcus is held up at the epithelial surface and that invasion leads to disease. Our data
334 are supported by murine colonisation experiments[38,39] and the detection of pneumococcal DNA in
335 blood of otherwise healthy, colonised children[40]. In line with other cell culture and murine
336 models[13,16,38,41], we have demonstrated that pneumococcal micro-invasion occurs by endocytosis
337 through the formation of cytoplasmic vacuoles, and by paracellular transcytosis across the
338 epithelium. This process appears to be association with the formation of epithelial folds different from
339 the membrane ruffles previously reported with conventionally intracellular pathogens such as
340 *Salmonella* typhimurium[42]. Our study emphasises the active nature of these processes without
341 marked cellular damage or loss of barrier function. Micro-invasion of the epithelium may overcome
342 the inaccessibility of PAMP receptors located either at the epithelial basolateral surface or
343 intracellularly[43,44]. We have found that at early time points, micro-invasion *in vitro* is also
344 characterised by pneumococcal co-association with JAM-A and β catenin without evidence of barrier
345 dysfunction. In murine models at later time points, TLR-dependent Claudin 7 and Claudin 10 down-
346 regulation enhanced pneumococcal translocation across the epithelium has been observed[13]. While
347 this may occur as inflammation becomes more prominent, our data suggest that micro-invasion can
348 happen without barrier disruption and that the epithelium plays an active role in the regulation of

349 these complex host-pathogen interactions[12]. How micro-invasion relates to the risk of invasive
350 pneumococcal disease remains to be determined but as demonstrated by the EHPC model, micro-
351 invasion may occur in healthy individuals without symptoms.

352

353 The differential impact of micro-invasion on the epithelial transcriptomic response was striking with
354 considerable enrichment of multiple diverse transcription factors and signalling pathways related to
355 innate immunity with the most invasive pneumococcal strains. The interactome module highlights
356 that although enrichment of gene activation in response to all pneumococcal strains is apparent (the
357 core module), a more diverse range of epithelial gene activation occurs between strains, reflecting
358 specific host-pathogen interactions. Nasal colonisation in murine models is proinflammatory[45,46], but
359 our *in vitro* and EHPC experiments with serotype 6B suggests this is not always the case, whereby
360 pneumococcal-host cell adherence, growth, endocytosis and paracellular migration can be
361 established without a marked host response. In the EHPC, clearance occurred around the time the
362 epithelial transcriptomic response was most prominent. Weiser and colleagues argue that the
363 colonising pneumococcus induces a host inflammatory response that mediates clearance, but also
364 promotes nutrient acquisition, mucus production and onward transmission[14,18,47], which is supported
365 by murine models[48] and epidemiological studies of viral-coinfection[49]. It has been suggested that
366 pneumolysin induces neutrophil influx and degranulation, leading to increased secretions from the
367 nasopharynx, so promoting transmission[5,18]. We therefore suggest that the epithelial innate response
368 resulting from pneumococcal colonisation could promote both clearance and transmission.

369

370 The enrichment of binding sites for the transcription factor KLF4 transcription factors seen in our *in*
371 *vitro* data suggests a counter-regulatory process aimed at minimising inflammation. KLF4 plays a
372 role in barrier function, suppression of NFκB-dependent IL-8 secretion, regulation of IL-10 expression
373 via TLR9-MyD88 and Yes-1, in response to *S. pneumoniae,* which is partially dependent on autolysin
374 LytA[32,50,51]. Thus, by exploiting micro-invasion, the pneumococcus may carefully calibrate the host
375 innate immune/ inflammatory response to promote survival through transmission.

376

377 A range of pneumococcal PAMPs including pneumolysin, may trigger this epithelial sensing
378 process[18,52]. We found pneumolysin to be a prominent inducer of epithelial surface molecule
379 upregulation, cytokine production and transcriptomic inflammatory response *in vitro*. Following
380 internalisation of the pneumococcus by neutrophils, pneumolysin has been shown to induce ROS
381 following bacterial autolysis, which leads to cellular activation[53]. We speculate that pneumolysin
382 released intracellularly may signal directly in epithelial cells or through host cell pore-formation
383 leading to entry of other PAMPs. Mediated by autolysin, the pneumococcus undergoes autolysis
384 during stationery growth phase, resulting in additional PAMPs' release including bacterial DNA[53]. In
385 mice, pneumococcal DNA triggers inflammation through a DAI/STING/TBK1/IRF3 cascade[45,54], a
386 response that may contribute to pneumococcal clearance. In our *in vitro* transcriptomic analyses, we
387 detected enriched activation of IRF3/IFR7 in dPly-TIGR4. We suggest that in the context of micro-
388 invasion, pneumococcal DNA may also act as a trigger of epithelial sensing, inducing inflammation[54].

389

390 Our findings are limited by the pneumococcal strains available for testing in the EHPC model to
391 enable direct comparisons with *in vitro* data. Nonetheless, the use of different strains *in vitro* has
392 enabled us and others[55,56] to determine the impact of different patterns of epithelial adherence and
393 invasion on the host inflammatory/ innate immune response. Currently, the EHPC model does not
394 allow us to definitively assess human to human transmission although the appropriate methods are
395 under development.

396

397 In conclusion, our data implicates the novel finding of micro-invasion during pneumococcal
398 colonisation of otherwise healthy humans, promoting epithelial-derived innate immunity/
399 inflammation and ultimately clearance. The pathways critical for onward pneumococcal transmission
400 remain to be determined in humans but based on murine models, we propose that this epithelial
401 response may also facilitate transmission. The balance between innate immunity/ inflammation-
402 driven transmission and clearance may be further modulated by the frequency of carriage events,
403 pneumococcal strain co-colonisation, viral co-infections and other environmental pressures[1,22,48].

404 Our approach combining *in vitro* with *in vivo* human systems offers a potentially tractable way to
405 further interrogate these processes.

406

407

408 **ACKNOWLEDGEMENTS**

409 This study was funded by the Wellcome Trust (Grant 106846/Z/15/Z). DF is supported by the Medical
410 Research Council (grant MR/M011569/1), Bill and Melinda Gates Foundation (grant OPP1117728)
411 and the National Institute for Health Research (NIHR) Local Comprehensive Research Network. The
412 authors wish to thank the EHPC Clinical Team at LSTM and all the volunteers. Confocal imaging
413 facilities at LSTM were funded by a Wellcome Trust Multi-User Equipment Grant (104936/Z/14/Z).
414 Flow cytometric acquisition at LSTM was funded by a Wellcome Trust Multi-User Equipment Grant
415 (104936/Z/14/Z). LytA PCR was performed by Prof. D Bogaert, University of Edinburgh, UK. For *in*
416 *vitro* data, RNAseq library preparation was undertaken at UCL through the UCL/UCLH Biomedical
417 Research Centre and MRC funded Pathogen Genomics Unit (G0900950). For the *in vivo* data,
418 RNAseq library preparation was performed and by Carl Anderson at the Wellcome Sanger Institute,
419 Hinxton. EM was performed by Dr. Mark Turmaine in the Biosciences EM facility at UCL.

420

421 **AUTHOR CONTRIBUTIONS**: CMW, SPJ, DMF and RSH conceived and designed the study. CMW,
422 SP, SPJ, JR, EN, CS acquired the data. CMW, CV, SPJ, MN, JSB, DMF, RSH analysed and
423 interpreted the data. CMW wrote the first draft of the manuscript. CMW, CV, SP, SPJ, JR, EN, CS,
424 MN, JSB, DMF, RSH commented on and approved the manuscript.

425

426 **COMPETING INTERESTS:** The authors declare no competing financial interests.

427

428

429

430

431

432 **REFERENCES**

433
434

435 1 O'Brien, K. L. *et al.* Burden of disease caused by Streptococcus pneumoniae in children younger than
436 5 years: global estimates. *Lancet* **374**, 893-902, doi:10.1016/S0140-6736(09)61204-6 (2009).
437 2 Whitney, C. G. *et al.* Decline in invasive pneumococcal disease after the introduction of protein-
438 polysaccharide conjugate vaccine. *N Engl J Med* **348**, 1737-1746, doi:10.1056/NEJMoa022823 (2003).
439 3 Hanage, W. P. *et al.* Carried pneumococci in Massachusetts children: the contribution of clonal
440 expansion and serotype switching. *Pediatr Infect Dis J* **30**, 302-308,
441 doi:10.1097/INF.0b013e318201a154 (2011).
442 4 Jochems, S. P., Weiser, J. N., Malley, R. & Ferreira, D. M. The immunological mechanisms that control
443 pneumococcal carriage. *PLoS Pathog* **13**, e1006665, doi:10.1371/journal.ppat.1006665 (2017).
444 5 Diavatopoulos, D. A. *et al.* Influenza A virus facilitates Streptococcus pneumoniae transmission and
445 disease. *FASEB J* **24**, 1789-1798, doi:10.1096/fj.09-146779 (2010).
446 6 Pido-Lopez, J., Kwok, W. W., Mitchell, T. J., Heyderman, R. S. & Williams, N. A. Acquisition of
447 pneumococci specific effector and regulatory Cd4+ T cells localising within human upper respiratory-
448 tract mucosal lymphoid tissue. *PLoS Pathog* **7**, e1002396, doi:10.1371/journal.ppat.1002396 (2011).
449 7 Zhang, Q. *et al.* Characterisation of regulatory T cells in nasal associated lymphoid tissue in children:
450 relationships with pneumococcal colonization. *PLoS Pathog* **7**, e1002175,
451 doi:10.1371/journal.ppat.1002175 (2011).
452 8 Pennington, S. H. *et al.* Polysaccharide-Specific Memory B Cells Predict Protection against
453 Experimental Human Pneumococcal Carriage. *Am J Respir Crit Care Med* **194**, 1523-1531,
454 doi:10.1164/rccm.201512-2467OC (2016).
455 9 Mitsi, E. *et al.* Agglutination by anti-capsular polysaccharide antibody is associated with protection
456 against experimental human pneumococcal carriage. *Mucosal Immunol* **10**, 385-394,
457 doi:10.1038/mi.2016.71 (2017).
458 10 Ratner, A. J., Lysenko, E. S., Paul, M. N. & Weiser, J. N. Synergistic proinflammatory responses induced
459 by polymicrobial colonization of epithelial surfaces. *Proc Natl Acad Sci U S A* **102**, 3429-3434,
460 doi:10.1073/pnas.0500599102 (2005).
461 11 Eisele, N. A. & Anderson, D. M. Host Defense and the Airway Epithelium: Frontline Responses That
462 Protect against Bacterial Invasion and Pneumonia. *J Pathog* **2011**, 249802, doi:10.4061/2011/249802
463 (2011).
464 12 Whitsett, J. A. & Alenghat, T. Respiratory epithelial cells orchestrate pulmonary innate immunity. *Nat*
465 *Immunol* **16**, 27-35, doi:10.1038/ni.3045 (2015).
466 13 Clarke, T. B., Francella, N., Huegel, A. & Weiser, J. N. Invasive bacterial pathogens exploit TLR-
467 mediated downregulation of tight junction components to facilitate translocation across the
468 epithelium. *Cell Host Microbe* **9**, 404-414, doi:10.1016/j.chom.2011.04.012 (2011).
469 14 Weiser, J. N., Ferreira, D. M. & Paton, J. C. Streptococcus pneumoniae: transmission, colonization and
470 invasion. *Nat Rev Microbiol* **16**, 355-367, doi:10.1038/s41579-018-0001-8 (2018).
471 15 Agarwal, V., Asmat, T. M., Dierdorf, N. I., Hauck, C. R. & Hammerschmidt, S. Polymeric
472 immunoglobulin receptor-mediated invasion of Streptococcus pneumoniae into host cells requires a
473 coordinate signaling of SRC family of protein-tyrosine kinases, ERK, and c-Jun N-terminal kinase. *J Biol*
474 *Chem* **285**, 35615-35623, doi:10.1074/jbc.M110.172999 (2010).
475 16 Asmat, T. M., Agarwal, V., Saleh, M. & Hammerschmidt, S. Endocytosis of Streptococcus pneumoniae
476 via the polymeric immunoglobulin receptor of epithelial cells relies on clathrin and caveolin
477 dependent mechanisms. *Int J Med Microbiol* **304**, 1233-1246, doi:10.1016/j.ijmm.2014.10.001
478 (2014).
479 17 Ratner, A. J., Aguilar, J. L., Shchepetov, M., Lysenko, E. S. & Weiser, J. N. Nod1 mediates cytoplasmic
480 sensing of combinations of extracellular bacteria. *Cell Microbiol* **9**, 1343-1351, doi:10.1111/j.1462-
481 5822.2006.00878.x (2007).
482 18 Zafar, M. A., Wang, Y., Hamaguchi, S. & Weiser, J. N. Host-to-Host Transmission of Streptococcus
483 pneumoniae Is Driven by Its Inflammatory Toxin, Pneumolysin. *Cell Host Microbe* **21**, 73-83,
484 doi:10.1016/j.chom.2016.12.005 (2017).

485 19 Malley, R. *et al.* Recognition of pneumolysin by Toll-like receptor 4 confers resistance to
486 pneumococcal infection. *Proc Natl Acad Sci U S A* **100**, 1966-1971 (2003).
487 20 Ratner, A. J. *et al.* Epithelial cells are sensitive detectors of bacterial pore-forming toxins. *J Biol Chem*
488 **281**, 12994-12998, doi:10.1074/jbc.M511431200 (2006).
489 21 Ferreira, D. M. *et al.* Controlled human infection and rechallenge with Streptococcus pneumoniae
490 reveals the protective efficacy of carriage in healthy adults. *Am J Respir Crit Care Med* **187**, 855-864,
491 doi:10.1164/rccm.201212-2277OC (2013).
492 22 Jochems, S. P. *et al.* Inflammation induced by influenza virus impairs human innate immune control
493 of pneumococcus. *Nat Immunol* **19**, 1299-1308, doi:10.1038/s41590-018-0231-y (2018).
494 23 Wright, A. K. *et al.* Human nasal challenge with Streptococcus pneumoniae is immunising in the
495 absence of carriage. *PLoS Pathog* **8**, e1002622, doi:10.1371/journal.ppat.1002622 (2012).
496 24 Trevejo-Nunez, G., Elsegeiny, W., Conboy, P., Chen, K. & Kolls, J. K. Critical Role of IL-22/IL22-RA1
497 Signaling in Pneumococcal Pneumonia. *J Immunol* **197**, 1877-1883, doi:10.4049/jimmunol.1600528
498 (2016).
499 25 Fais, S. *et al.* HLA-DR antigens on colonic epithelial cells in inflammatory bowel disease: I. Relation to
500 the state of activation of lamina propria lymphocytes and to the epithelial expression of other surface
501 markers. *Clin Exp Immunol* **68**, 605-612 (1987).
502 26 Propst, S. M., Denson, R., Rothstein, E., Estell, K. & Schwiebert, L. M. Proinflammatory and Th2-
503 derived cytokines modulate CD40-mediated expression of inflammatory mediators in airway
504 epithelia: implications for the role of epithelial CD40 in airway inflammation. *J Immunol* **165**, 2214-
505 2221 (2000).
506 27 Cagnoni, F. *et al.* CD40 on adult human airway epithelial cells: expression and proinflammatory
507 effects. *J Immunol* **172**, 3205-3214 (2004).
508 28 Frick, A. G. *et al.* Haemophilus influenzae stimulates ICAM-1 expression on respiratory epithelial cells.
509 *J Immunol* **164**, 4185-4196 (2000).
510 29 Tettelin, H. *et al.* Complete genome sequence of a virulent isolate of Streptococcus pneumoniae.
511 *Science* **293**, 498-506, doi:10.1126/science.1061217 (2001).
512 30 Asmat, T. M., Agarwal, V., Rath, S., Hildebrandt, J. P. & Hammerschmidt, S. Streptococcus
513 pneumoniae infection of host epithelial cells via polymeric immunoglobulin receptor transiently
514 induces calcium release from intracellular stores. *J Biol Chem* **286**, 17861-17869,
515 doi:10.1074/jbc.M110.212225 (2011).
516 31 Peter, A. *et al.* Localization and pneumococcal alteration of junction proteins in the human alveolar-
517 capillary compartment. *Histochem Cell Biol* **147**, 707-719, doi:10.1007/s00418-017-1551-y (2017).
518 32 Herta, T. *et al.* DNA-release by Streptococcus pneumoniae autolysin LytA induced Krueppel-like
519 factor 4 expression in macrophages. *Sci Rep* **8**, 5723, doi:10.1038/s41598-018-24152-1 (2018).
520 33 Malley, R. *et al.* Recognition of pneumolysin by Toll-like receptor 4 confers resistance to
521 pneumococcal infection. *Proc Natl Acad Sci U S A* **100**, 1966-1971, doi:10.1073/pnas.0435928100
522 (2003).
523 34 Takahashi, S. *et al.* Pneumococcal Infection Aggravates Elastase-Induced Emphysema via Matrix
524 Metalloproteinase 12 Overexpression. *J Infect Dis* **213**, 1018-1030, doi:10.1093/infdis/jiv527 (2016).
525 35 Pollara, G. *et al.* Validation of Immune Cell Modules in Multicellular Transcriptomic Data. *PLoS One*
526 **12**, e0169271, doi:10.1371/journal.pone.0169271 (2017).
527 36 Schmeck, B. *et al.* Streptococcus pneumoniae induced c-Jun-N-terminal kinase- and AP-1 -dependent
528 IL-8 release by lung epithelial BEAS-2B cells. *Respir Res* **7**, 98, doi:10.1186/1465-9921-7-98 (2006).
529 37 Siegel, S. J. & Weiser, J. N. Mechanisms of Bacterial Colonization of the Respiratory Tract. *Annu Rev*
530 *Microbiol* **69**, 425-444, doi:10.1146/annurev-micro-091014-104209 (2015).
531 38 Mahdi, L. K., Ogunniyi, A. D., LeMessurier, K. S. & Paton, J. C. Pneumococcal virulence gene expression
532 and host cytokine profiles during pathogenesis of invasive disease. *Infect Immun* **76**, 646-657,
533 doi:10.1128/IAI.01161-07 (2008).
534 39 Briles, D. E., Novak, L., Hotomi, M., van Ginkel, F. W. & King, J. Nasal colonization with Streptococcus
535 pneumoniae includes subpopulations of surface and invasive pneumococci. *Infect Immun* **73**, 6945-
536 6951, doi:10.1128/IAI.73.10.6945-6951.2005 (2005).

537 40 Morpeth, S. C. *et al.* Detection of Pneumococcal DNA in Blood by Polymerase Chain Reaction for
538 Diagnosing Pneumococcal Pneumonia in Young Children From Low- and Middle-Income Countries.
539 *Clin Infect Dis* **64**, S347-S356, doi:10.1093/cid/cix145 (2017).
540 41 Talbot, U. M., Paton, A. W. & Paton, J. C. Uptake of Streptococcus pneumoniae by respiratory
541 epithelial cells. *Infect Immun* **64**, 3772-3777 (1996).
542 42 Jones, B. D., Paterson, H. F., Hall, A. & Falkow, S. Salmonella typhimurium induces membrane ruffling
543 by a growth factor-receptor-independent mechanism. *Proc Natl Acad Sci U S A* **90**, 10390-10394
544 (1993).
545 43 Gewirtz, A. T., Navas, T. A., Lyons, S., Godowski, P. J. & Madara, J. L. Cutting edge: bacterial flagellin
546 activates basolaterally expressed TLR5 to induce epithelial proinflammatory gene expression. *J*
547 *Immunol* **167**, 1882-1885 (2001).
548 44 Hornef, M. W., Wick, M. J., Rhen, M. & Normark, S. Bacterial strategies for overcoming host innate
549 and adaptive immune responses. *Nat Immunol* **3**, 1033-1040, doi:10.1038/ni1102-1033 (2002).
550 45 Koppe, U. *et al.* Streptococcus pneumoniae stimulates a STING- and IFN regulatory factor 3-
551 dependent type I IFN production in macrophages, which regulates RANTES production in
552 macrophages, cocultured alveolar epithelial cells, and mouse lungs. *J Immunol* **188**, 811-817,
553 doi:10.4049/jimmunol.1004143 (2012).
554 46 Wilson, R. *et al.* Protection against Streptococcus pneumoniae lung infection after nasopharyngeal
555 colonization requires both humoral and cellular immune responses. *Mucosal Immunol* **8**, 627-639,
556 doi:10.1038/mi.2014.95 (2015).
557 47 Zafar, M. A., Kono, M., Wang, Y., Zangari, T. & Weiser, J. N. Infant Mouse Model for the Study of
558 Shedding and Transmission during Streptococcus pneumoniae Monoinfection. *Infect Immun* **84**,
559 2714-2722, doi:10.1128/IAI.00416-16 (2016).
560 48 Plotkowski, M. C., Puchelle, E., Beck, G., Jacquot, J. & Hannoun, C. Adherence of type I Streptococcus
561 pneumoniae to tracheal epithelium of mice infected with influenza A/PR8 virus. *Am Rev Respir Dis*
562 **134**, 1040-1044, doi:10.1164/arrd.1986.134.5.1040 (1986).
563 49 Pittet, L. A., Hall-Stoodley, L., Rutkowski, M. R. & Harmsen, A. G. Influenza virus infection decreases
564 tracheal mucociliary velocity and clearance of Streptococcus pneumoniae. *Am J Respir Cell Mol Biol*
565 **42**, 450-460, doi:10.1165/rcmb.2007-0417OC (2010).
566 50 Zahlten, J. *et al.* Role of Pneumococcal Autolysin for KLF4 Expression and Chemokine Secretion in
567 Lung Epithelium. *Am J Respir Cell Mol Biol* **53**, 544-554, doi:10.1165/rcmb.2014-0024OC (2015).
568 51 Zahlten, J. *et al.* TLR9- and Src-dependent expression of Krueppel-like factor 4 controls interleukin-
569 10 expression in pneumonia. *Eur Respir J* **41**, 384-391, doi:10.1183/09031936.00196311 (2013).
570 52 Hotomi, M., Yuasa, J., Briles, D. E. & Yamanaka, N. Pneumolysin plays a key role at the initial step of
571 establishing pneumococcal nasal colonization. *Folia Microbiol (Praha)* **61**, 375-383,
572 doi:10.1007/s12223-016-0445-z (2016).
573 53 Martner, A., Dahlgren, C., Paton, J. C. & Wold, A. E. Pneumolysin released during Streptococcus
574 pneumoniae autolysis is a potent activator of intracellular oxygen radical production in neutrophils.
575 *Infect Immun* **76**, 4079-4087, doi:10.1128/IAI.01747-07 (2008).
576 54 Parker, D. *et al.* Streptococcus pneumoniae DNA initiates type I interferon signaling in the respiratory
577 tract. *MBio* **2**, e00016-00011, doi:10.1128/mBio.00016-11 (2011).
578 55 Bootsma, H. J., Egmont-Petersen, M. & Hermans, P. W. Analysis of the in vitro transcriptional
579 response of human pharyngeal epithelial cells to adherent Streptococcus pneumoniae: evidence for
580 a distinct response to encapsulated strains. *Infect Immun* **75**, 5489-5499, doi:10.1128/IAI.01823-06
581 (2007).
582 56 Novick, S. *et al.* Adhesion and invasion of Streptococcus pneumoniae to primary and secondary
583 respiratory epithelial cells. *Mol Med Rep* **15**, 65-74, doi:10.3892/mmr.2016.5996 (2017).
584 57 Browall, S. *et al.* Intraclonal variations among Streptococcus pneumoniae isolates influence the
585 likelihood of invasive disease in children. *J Infect Dis* **209**, 377-388, doi:10.1093/infdis/jit481 (2014).
586 58 McCool, T. L., Cate, T. R., Moy, G. & Weiser, J. N. The immune response to pneumococcal proteins
587 during experimental human carriage. *J Exp Med* **195**, 359-365 (2002).

588 59 Hyams, C., Camberlein, E., Cohen, J. M., Bax, K. & Brown, J. S. The Streptococcus pneumoniae capsule
589 inhibits complement activity and neutrophil phagocytosis by multiple mechanisms. *Infect Immun* **78**,
590 704-715, doi:10.1128/IAI.00881-09 (2010).
591 60 Collins, A. M. *et al.* First human challenge testing of a pneumococcal vaccine. Double-blind
592 randomized controlled trial. *Am J Respir Crit Care Med* **192**, 853-858, doi:10.1164/rccm.201503-
593 0542OC (2015).
594 61 Jochems, S. P. *et al.* Novel Analysis of Immune Cells from Nasal Microbiopsy Demonstrates Reliable,
595 Reproducible Data for Immune Populations, and Superior Cytokine Detection Compared to Nasal
596 Wash. *PLoS One* **12**, e0169805, doi:10.1371/journal.pone.0169805 (2017).
597 62 Bray, N. L., Pimentel, H., Melsted, P. & Pachter, L. Near-optimal probabilistic RNA-seq quantification.
598 *Nat Biotechnol* **34**, 525-527, doi:10.1038/nbt.3519 (2016).
599 63 Soneson, C., Love, M. I. & Robinson, M. D. Differential analyses for RNA-seq: transcript-level
600 estimates improve gene-level inferences. *F1000Res* **4**, 1521, doi:10.12688/f1000research.7563.2
601 (2015).
602 64 Varet, H., Brillet-Gueguen, L., Coppee, J. Y. & Dillies, M. A. SARTools: A DESeq2- and EdgeR-Based R
603 Pipeline for Comprehensive Differential Analysis of RNA-Seq Data. *PLoS One* **11**, e0157022,
604 doi:10.1371/journal.pone.0157022 (2016).
605 65 Chakraborty, S., Datta, S. & Datta, S. Surrogate variable analysis using partial least squares (SVA-PLS)
606 in gene expression studies. *Bioinformatics* **28**, 799-806, doi:10.1093/bioinformatics/bts022 (2012).
607 66 Fang, H., Knezevic, B., Burnham, K. L. & Knight, J. C. XGR software for enhanced interpretation of
608 genomic summary data, illustrated by application to immunological traits. *Genome Med* **8**, 129,
609 doi:10.1186/s13073-016-0384-y (2016).
610 67 Kwon, A. T., Arenillas, D. J., Worsley Hunt, R. & Wasserman, W. W. oPOSSUM-3: advanced analysis
611 of regulatory motif over-representation across genes or ChIP-Seq datasets. *G3 (Bethesda)* **2**, 987-
612 1002, doi:10.1534/g3.112.003202 (2012).

613
614
615
616
617

618 **METHODS**

619

620 **Bacteria**

621 *S. pneumoniae* clinical strains used were 6B (BHN 418[57]), 23F (P1121[58]) and TIGR4 (P1672[59]),
622 together with a pneumolysin deficient TIGR4 mutant strain (P1672, a kind gift from Prof T Mitchell,
623 University of Birmingham). Stocks of bacterial aliquots grown to $O.D._{600nm}$ 0.3 were stored at -80°C,
624 defrosted, resuspended in cell culture media and used once. Colony forming units (CFU) were
625 counted on horse blood agar plates (EO Labs).

626

627 **Experimental Human Pneumococcal Carriage Model (EHPC)**

628 Following written informed consent, healthy non-smoking adults between the ages of 18 – 59 were
629 inoculated with 80,000 CFU/nostril live 6B *S. pneumoniae* (BHN418), grown to mid-log phase in

630 vegetone broth as previously described[60]. Individuals naturally colonised with *S. pneumoniae* or in
631 regular contact with at-risk individuals were excluded (except for EM images in Supplementary
632 Figure 1b). Blood and mucosal T cell and antibody immunity were not systematically measured in
633 this cohort but previous studies of volunteers from this population have demonstrated background T
634 cell and antibody-mediated anti-pneumococcal immunity, but a relationship between pre-challenge
635 immunity and the development of carriage in the model has not been established[21,23]. To exclude
636 the influence of viral-coinfection, EHPC model volunteers who had coryzal or flu-like symptoms prior
637 to challenge were excluded. Volunteers were screened for the presence of 20 common respiratory
638 viruses before inoculation. 1/13 asymptomatic volunteers (volunteer 1) was positive for enterovirus.
639 Nasal washes and mucosal cells (curette biopsy) from the inferior turbinate were obtained by PBS
640 syringe and curettage using a plastic Rhino-probe™ (Arlington Scientific), in this order of collection
641 respectively, before pneumococcal inoculation. Sampling was then repeated on days 2, 6, 9, and 14
642 - 27 post pneumococcal inoculation[61]. Volunteers received the TIV vaccine intramuscularly at day 3
643 post pneumococcal inoculation. Bacteria collected from nasal washes were quantified by CFU
644 counts. At each time-point, two curettage samples were obtained and processed for confocal
645 immunofluorescence, flow cytometry, primary cell culture and /or transcriptomic analysis by RNA
646 sequencing (RNAseq). There were no adverse events. The carriage status of each volunteer was
647 blinded until sample analysis was completed.
648
649 Ethical approval was given by NHS Research and Ethics Committee (REC)/Liverpool School of
650 Tropical Medicine (LSTM) REC, reference numbers: 15/NW/0146 and 14/NW/1460 and Human
651 Tissue Authority licensing number 12548.
652
653 **Human Respiratory Tract Epithelial Cell Lines**
654 Human pharyngeal carcinoma Detroit 562 epithelial cells (ATCC_CCL-138) and human bronchial
655 carcinoma Calu3 epithelial cells (ATCC_HTB-55) were grown in 10% FCS in alpha MEM media
656 (Gibco). Human alveolar epithelial carcinoma A549 epithelial cells (ATCC_CCL-185) were grown in
657 10% FCS with 1% L-glutamine in Hams/F-12 media (Gibco).

658

659 **Pneumococcal-epithelial cell co-culture**

660 *Association and Invasion assays* - confluent Detroit 562 (typically day 8 post plating), Calu3 (typically
661 day 10 post plating) and A549 (typically day 4 post plating) monolayers cultured on 12 well plates
662 (Corning), were exposed to *S. pneumoniae* for three hours in 1% FCS alpha MEM (~MOI
663 approximately 1 cell: 10 pneumococci). The medium was removed, and cells washed three times in
664 $HBSS^{+/+}$. Cells were incubated in 1% saponin for 10 minutes at 37°C and lysed by repetitive pipetting.
665 Dilutions of bacteria were plated on blood agar and colonies counted after 16 hours. To quantify
666 internalised bacteria, 100µg/ml gentamicin was added for 1 hour to the cells, which were washed
667 another three times, before incubating with 1% Saponin and plating on blood agar plates. CFUs were
668 counted after 16 hours incubation at 37°C, 5% CO_2. There were no differences in pneumococcal
669 pre- or post-inoculum, or growth density between the strains, in the cell supernatant three hours
670 post-infection.

671

672 *Transmigration assay* - Detroit 562 cells were cultured on 3µm pore, PET Transwell Inserts
673 (ThermoFisher) typically for 10 days to achieve confluent, polarised monolayers. Calu3 cells were
674 plated onto Transwell inserts typically for 12 days and A549 cells typically for 6 days. Cell culture
675 media was changed 1 hour prior to addition of bacteria to 1% FCS (250µl apical chamber, 1ml basal
676 chamber). Resistance was recorded before and after *S. pneumoniae* were added using an EVOM2
677 (World Precision Instruments). 1mg/ml FITC-dextran (Sigma Aldrich) was added to the apical
678 chamber of selected inserts to assess permeability. Approximately 12 million bacteria were added
679 to the cells (~MOI 1 cell: 25 bacteria). During the time course, 50µl was removed, diluted and plated,
680 from the basal chamber to measure bacterial load by counting CFU/well. Permeability was recorded
681 using a FLUOstar Omega (BMG Labtech) at 488nm.

682

683 *Endocytosis inhibition assays* - Detroit 562 cells cultured on 12 well plates were treated with 100µM
684 dynasore (Cambridge Biosciences) and 7.5µg/ml nystatin (Sigma Aldrich) to block endocytosis for
685 30 minutes prior to, and for the duration of pneumococcal infection incubation period. DMSO was

686 used as a control. Cells were washed and treated with gentamicin and lysed with saponin as
687 described above.
688
689 **Confocal Microscopy**
690 For the *in vivo* analysis, mucosal cells derived by curettage from the EHPC model were placed
691 directly into 4% PFA for 1 hour. Cells were cytospun onto microscope slides and allowed to air dry.
692 For the *in vitro* analysis, epithelial cell lines on transwell membranes were fixed in either 4% PFA
693 (Pierce, Methanol Free) or 1:1 mix of methanol: acetone for 20 minutes. For both *in vivo* and *in vitro*
694 samples, cells were permeabilised with 0.2% Triton X-100 for 10 minutes and blocked for 1 hour in
695 blocking buffer (3% goat serum and 3% BSA in PBS) before incubation with either pneumococcal
696 antisera Pool Q (for 6B or 23F detection, SSI Diagnostica), or pneumococcal antisera Type 4 (for
697 TIGR4 and dPly detection, SSI Diagnostica) to detect pneumococci, and JAM-A, Claudin-4 or β-
698 catenin primary antibodies to detect cellular junctional proteins (see Supplementary Information) for
699 one hour and then secondary and/or conjugated antibodies for 45 minutes. DAPI solution was added
700 for 5 minutes. After washing, the stained samples were mounted using Aqua PolyMount (VWR
701 International) with a coverslip onto a microslide. The entire cytospin for each sample was manually
702 viewed by microscopy for detection of pneumococci. Multiple fields of view (>3) were imaged for
703 each transwell insert, for each condition. Images were captured using either an inverted LSM 700,
704 LSM 880, or TissueFAXS Zeiss Confocal Microscope. Z stacks were recorded at 1μm intervals at
705 either 40x oil or 63x oil objectives. For the *in vivo* samples, the operator (CMW) was blinded to the
706 colonisation status of the volunteer at the time of sampling.
707
708 **Electron Microscopy**

709 Detroit 562 cells cultured on either transwells (scanning EM) or coverslips (transmission EM)
710 were fixed with 2% paraformaldehyde and 1.5% glutaraldehyde in 0.1 M cacodylate buffer
711 and post-fixed in 1% OsO4 / 1.5% K4Fe(CN)6 in 0.1 M cacodylate buffer pH7.3. Samples
712 were dehydrated in graded ethanol-water series and infiltrated with Agar 100 resin mix.
713 Ultra-thin sections were cut at 70-80 nm using a diamond knife on a Reichert ultracut

714 microtome. Sections were collected on 300 mesh copper grids and stained with lead citrate.
715 Samples were viewed in a Joel 1010 transition electron microscope and images recorded
716 using a Gatan Orius camera. Further details of TEM and SEM methods can be found in the
717 Supplementary information.

718

719 **Flow cytometry**

720 For the *in vivo* analysis, cells from two curette samples were incubated in cold PBS++ (PBS
721 supplemented with 5mM EDTA and 0.5% FCS) were dislodged by pipetting and centrifuged at 440g
722 for 5 mins at 4°C. Supernatant was removed, and cells resuspended in 25µl of PBS++ with
723 Live/Dead™ Fixable Violet Dead Cell Stain (ThermoFisher). After 15 minutes incubation on ice, an
724 antibody cocktail to stain for epithelial surface marker expression (see Supplementary Information)
725 was added and incubated for another 15 minutes. Samples were vortexed, resuspended in 3.5mls
726 of PBS++ and filtered over a pre-wetted 70µm filter. Samples were transferred to a 5ml FACS tube,
727 centrifuged and resuspended in 200µl Cell Fix (BD Biosciences) and acquired on LSRII Flow
728 Cytometer (BD Biosciences). Compensation was run and applied for each experimental replicate
729 and voltages consistent throughout. Isotype controls (Biolegend) and FL-1 controls were also run for
730 each antibody. Analyses of data was performed using FlowJo LLC version 10 software. Data was
731 performed on the gated epithelial cell population and only samples containing 500 or more cells are
732 reported.

733

734 For the *in vitro* analysis, confluent monolayers of Detroit 562 cells on 6 well plates were incubated
735 with *S. pneumoniae* for 6 hours in 1% FCS phenol free alpha MEM (base media, Life Technologies).
736 Cells were washed three times in PBS and gently lifted from the plate using a cell scraper in 300µl
737 of base media supplemented with 1mM EDTA. Samples were transferred to 5ml FACS tubes and
738 placed on ice for the duration of the protocol. Each cell sample was incubated with an antibody
739 cocktail for epithelial surface marker expression (see Supplemental Information) and Live/Dead™
740 Fixable Zombie Blue UV Cell Stain (Biolegend) for 30 minutes before rinsing in 1ml base media and
741 centrifuging at 300g for 5 minutes at 4°C. Cells were fixed in 600µl of 4% PFA and acquired on an

742 LSR II Flow Cytometer (BD Biosciences). Compensation was run and applied for each experimental
743 replicate and voltages consistent throughout. Isotype controls (BD Biosciences), FL-1 and single
744 stains were also run for each experiment. Samples were acquired until 300,000 events had been
745 collected. Analyses were performed using FlowJo LLC version 10 software.
746
747
748 **ELISAs**
749 Supernatant from Detroit 562 cells that had been incubated with *S. pneumoniae* for 6 hours, was
750 collected for cytokine analysis. IL-6, IL-8 and ICAM-1 DuoSet® ELISA kits were purchased from
751 R&D Systems and protocol followed according to manufacturers' instructions.
752
753 **RNA samples and sequencing (RNASeq)**

754 Mucosal curettage samples and epithelial cell cultures (incubated with or without *S. pneumoniae* for
755 3 hours) were collected in RNALater (ThermoFisher) and stored at -80°C. RNA Extraction was
756 performed using the RNEasy micro kit (Qiagen) and genomic DNA was removed with on column
757 DNA digestion or with the Turbo DNA-free Kit (Qiagen). Extracted RNA quality was assessed and
758 quantified using a BioAnalyser (Agilent 2100). For mucosal curettage samples, library preparation
759 and RNA-sequencing (Illumina Hiseq 4000, 15 lanes in total with 7 samples per lane, 100bp and
760 75bp paired-end reads) were performed at the Beijing Genome Institute (China) or the Wellcome
761 Sanger Institute (UK), respectively. For the Detroit 562 samples, library preparation was performed
762 using the Kappa Hyperprep kit (Roche Diagnostics) and sequencing was undertaken by the
763 Pathogens Genomic Unit (UCL) on the Illumina Nextseq using the Nextseq 500/550 High Output 75
764 cycle kit (Illumina) according to manufacturers' instructions, giving 15-20 million 41bp paired end
765 reads per sample.

766

767 All data processing and analysis was conducted in R, language and environment for statistical
768 computing (https://www.R-project.org). Paired end reads were mapped to the Ensembl human

769 transcriptome reference sequence (homo sapiens GRCh38). Mapping and generation of read counts
770 per transcript were performed using Kallisto[62], based on pseudoalignment. R/Bioconductor package
771 Tximport was used to import the mapped counts data and summarise the transcripts-level data into
772 gene level data[63]. DESeq2 and SARTools packages[64], were used for differential gene expression
773 analysis, using a false discovery rate (FDR) <0.05, following normalisation with a negative binomial
774 generalised linear model. In addition, transcript abundance for protein coding genes was expressed
775 as $\log_2$-transformed transcripts per million (TPM) by normalising the read counts to gene length and
776 then read depth. Transcriptomes from nasal samples ranged from 16 to 66 million reads per sample
777 and in principle component analysis, revealed a batch effect that was corrected by the Combat
778 function in the Surrogate Variable Analysis (SVA) R/Bioconductor package[65].

779

780 Identification of interacting networks and pathway enrichment analysis was performed using XGR R
781 package[66]. Interacting genes (supported by at least one experimental source of evidence) were
782 identified from the Pathway Commons database for directed interactions. These were then subjected
783 to Reactome pathway enrichment analysis with FDR<0.05. K-means clustering of Jaccard indices
784 to quantify similarity between the composition of genes mapping to each pathway was used to
785 identify 20 groups of pathways, from which the pathway consisting of the largest total number of
786 genes was selected to provide a representative annotation for each group. Transcription factor
787 binding site enrichment analysis was performed using the human single site analysis function in
788 oPOSSUM[67]. The expression of gene modules in the nasal transcriptomes was represented by the
789 mean Log_2 TPM value of the genes in each module.

790

791 **Code and RNAseq data availability**

792 Codes used to process the RNAseq data can be found at https://github.com/cristina86cristina.
793 RNAseq data from the EHPC are accessible through GEO Series Number GSE124949. RNAseq
794 data from the Detroit 562 cell infections is accessible through the ArrayExpress database at EMBL-
795 EBI under accession number E-MTAB-7841. Data from differential gene expression from

796 upregulated genes following infection, Reactome pathways and transcription factor analysis can be
797 found in Supplemental Excel Files 1 - 4.

798

799 **Statistics**

800 All experiments were conducted with replicates in three or more independent experiments unless
801 stated otherwise. Error bars represent SEM unless stated otherwise. GraphPad Prism Version 10
802 was used to perform two-tailed parametric (t-tests or ANOVA) or non-parametric (Mann-Whitney or
803 Kruskal-Wallis tests) analysis, which was based on the Shapiro-Wilk normality test. P values less
804 than 0.05 were considered significant and are derived from non-parametric statistical tests unless
805 stated otherwise.

806

807

808

809

810

811

812 **FIGURE LEGENDS**

813

814 **Table 1. *Streptococcus pneumoniae* association with the nasal epithelium in the EHPC model**
815 **detected by culture, confocal microscopy and LytA PCR**

816 Nasal washes and nasal curette biopsies were collected from carriage positive and carriage negative
817 volunteers over time. Standard methods for measuring bacterial density by culture (CFU) and LytA
818 PCR were compared against counts visualised by confocal microscopy for pneumococcal
819 association with nasal cells over time. The data was derived from 13 volunteers. + (1-10
820 pneumococci); ++ (11-50 pneumococci); +++ (51-100 pneumococci); ++++ (>100 pneumococci); n/a
821 = reading not taken.

822

823 **Figure 1. *Streptococcus pneumoniae* colonisation of the human nasal epithelium from the**
824 **EHPC model is associated with adhesion, micro-colony formation and micro-invasion in**
825 **response to *S. pneumoniae* 6B colonisation**

826 (a) Representative fields from the EHPC model nasal curette biopsies show intact epithelium can be
827 obtained from the samples (as visualised by XY planes) and they retain their size and shape (as
828 visualised by XZ planes). Cells were stained with Wheat Germ Agglutinin (WGA) or Junctional
829 Adhesion Molecule -A (JAM-A, red) and nuclei (blue). (b) The pattern of pneumococcal density
830 detected by culture and microscopy. (c) The proportion of bacteria located on the cell surface,
831 intracellularly, or paracellularly visualised by confocal microscopy, quantified from 8 volunteers
832 collected over time from microscopy counts. (d) Cells were stained for surface carbohydrates using
833 WGA (red), and the bacteria were marked with specific serotype antiserum (green). XY images of
834 1µm slices through a layer of cells from top (stack 1) to bottom (stack 4), with bacteria associated.
835 (e) Examples of cells collected on day 6 post-inoculation stained with WGA (red) showing; (ei)
836 mMicro-colony formation on the surface of the epithelium, (eii) bacterial internalization, (eiii)
837 migration through epithelial uptake internally or between cells. (f) Co-association between *S.*
838 *pneumoniae* (green) and JAM-A (red). Nuclei (blue). Bacterial uptake appeared co-associated with
839 JAM-A (yellow).

840

841 **Figure 2. Epithelial surface marker expression is not altered in response *to S. pneumoniae***
842 **6B colonisation *in vivo***

843 Epithelial cells from nasal curette biopsies were analysed by flow cytometry for (a) CD54 and (b)
844 CD107a. Results were expressed as median fluorescence intensity (left) and high cell surface
845 expression (≥95% of the baseline expression, right) representing at least two volunteers per time
846 point who were carriage negative (black) and carriage positive (grey). Comparisons between
847 carriage negative and carriage positive, on each day of sampling, was analysed by 1-way ANOVA
848 (a – parametric, b – non-parametric). P = 0.84 CD54 MFI; p = 0.98 CD54 %; p = 0.09 CD107a MFI;
849 p = 0.10 CD107a %.

850

851 **Figure 3. *Streptococcus pneumoniae* infection of nasopharyngeal epithelium *in vitro* is**
852 **associated with adhesion, micro-colony formation, micro-invasion, transmigration and is**
853 **partially influenced by pneumolysin.**

854 (a) Pneumococcal association and (b) internalisation: Detroit 562 cell monolayers were stimulated
855 with pneumococci for 1 or 3 hours and the quantity of associated bacteria was determined by culture
856 (CFU); n = 6. ****P = <0.0001, ***P = 0.0001: - (a) 1hr (dashed lines, ANOVA); 3hr (solid lines,
857 Kruskall-Wallis); (b) (Kruskall-Wallis). (c) Pneumococcal transmigration: Cells on transwell inserts
858 were stimulated with pneumococci for 3 hours and bacterial density in the basal chamber was
859 determined (**P = 0.0092, Kruskall-Wallis). N = 5. (d) Representative pneumococcal-density (green)
860 images of cells (blue nuclei). Scale bar = 20µm. n = 5. (e - h) Representative images of
861 pneumococcal localization (green) from cells (red, JAM-A), illustrating: (e) differences in adherence
862 by 6B and TIGR4; (f) internalised bacteria (top 6B; bottom TIGR4) co-localised with JAM-A with
863 associated intracellular vesicle-like bodies (yellow); (g) lateral localisation of pneumococci (XY
864 images, TIGR4) with possible paracellular movement co-associated with JAM-A (XZ images, 6B);
865 (h) basal localisation of bacteria (23F) at the level of nuclei and insert pores N = 5 with replicates. (i)
866 Scanning EM images of Detroit 562 cells infected with *S. pneumoniae* which appear as diplococci.
867 Left – pneumococcal chain formation (strain 23F, arrow); middle and right – micro-colony formation
868 by strains 6B and TIGR4 on the epithelial surface. (i) Micro-invasion of dPLY-TIGR4 shown by EM:
869 left - scanning EM showing epithelial membrane folding (arrows) and pneumococci below the cell
870 membrane surface (*); middle – internalisation of TIGR4 pneumococci encased within a vacuole
871 (arrow); and right – transmission EM showing transmigration of dPLY-TIGR4 pneumococci between
872 epithelial cells (arrow).

873

874 **Figure 4. Transmigration of *S. pneumoniae* is endocytosis-dependent but does not disrupt**
875 **barrier integrity or function**

876 (a and b) Detroit 562 cells were treated with dynasore and nystatin for 30 minutes prior to and during
877 incubation with 23F, for 1 hour. (a) Intracellular bacteria were quantified using a gentamicin
878 protection assay and CFUs counted (****P = <0.0001, Mann-Whitney). (b) Transmigrated bacteria
879 after one hour were counted by CFUs (*P = 0.013 Mann-Whitney). N = 4. (c and d) Cells were co-
880 infected with pneumococci for three hours on transwell inserts and barrier function was measured.
881 (c) Trans-Epithelial Electrical Resistance (TEER) was compared before and after exposure to
882 pneumococci. N = 9. Calcium withdrawal was used as a positive control (***P = 0.0013, unpaired T-
883 test, n = 3). (d) Permeability was assessed by leak to 4kDa FITC-dextran, collected from basal
884 chamber. N = 4. ****P = <0.0001 comparing non-infected against pneumococci (Kruskall-Wallis).
885 Blank inserts were used as a positive control (Mann-Whitney).

886

887 **Figure 5. Epithelial CD107a and CD54 surface expression and secretion of IL-6, IL-8 and CD54**
888 **are upregulated after *S. pneumoniae* exposure *in vitro***

889 (a and b) Detroit 562 cells were stimulated with *S. pneumoniae* for 6 hours and the median
890 fluorescence intensity and high-expressing cells for (a) CD54 and (b) CD107a were analysed by flow
891 cytometry. n = 3 independent experiments (**** P < 0.0001 CD107a MFI, compared to non-infected
892 cells, ANOVA. *** P = 0.0009 for MFI CD107a, TIGR4 v dPly, unpaired T-test. *** P < 0.001 CD107a
893 high expression, compared to non-infected cells, ANOVA *P = 0.028 for high expression CD107a,
894 TIGR4 vs. dPly, Mann-Whitney). (* P = 0.048 NI v TIGR4; * P = 0.0367 NI v dPly for CD54, ANOVA).

895 (c) IL-6, IL-8 and CD54 in the supernatants from Detroit 562 cells stimulated with *S. pneumoniae* for
896 6 hours, were measured by ELISA. N = 6 independent experiments with replicates. (**** P <0.0001
897 IL-6; *** P = 0.0013 CD54; **** P < 0.0001 IL-8 (Kruskall-Wallis test)).

898

899 **Figure 6. The epithelial transcriptomic response to *Streptococcus pneumoniae in vitro* is**
900 **influenced by epithelial adhesion and micro-invasion**

901 (a) The total number of Detroit 562 epithelial genes upregulated following exposure to 6B, 23F,
902 TIGR4 and TIGR4-dPly pneumococci, compared to non-infected samples. N = 3 independent
903 experiments with replicates. Genes with an FDR <0.05 were considered for further analysis. The
904 matrix shows intersections for the four strains, sorted by size. Dark circles in the matrix indicates
905 sets that are part of the intersection. (b) Bubble heat map showing the results of transcriptional factor
906 analysis in Opossum for each strain. Transcriptional factors are ordered by family and then sorted
907 by number of genes in the database. The colour represents the log2 z-scores (a continuum from
908 blue (lowest values) to red (highest values) and the size shows the number of genes annotated to
909 the particular pathway. (c) Bubble heat map showing the results of Reactome Pathway Analysis for
910 upregulated genes in each strain compared to non-infected cells. Pathways were clustered in 20
911 groups using K-means on Jaccard index and the biggest pathway for each group was selected for
912 representative annotation of each cluster. Individual pathways within clusters are shown in
913 Supplementary Figure 8. The colour represents the log2 z-scores (a continuum from blue (lowest
914 values) and red (highest values) and the size shows the number of genes annotated to each
915 pathway. (d) Selected bubble heat map clusters representing the individual pathways within each
916 cluster from (c).

917

918 **Figure 7. Epithelial-derived transcriptomic responses to *S. pneumoniae* in the EHPC model**
919 **co-incides with bacterial clearance**

920 (a) Network representation generated from the *in vitro* analyses for each strain. From the genes
921 present in the networks, an integrated gene list (200 genes) and a core genes list (16 genes) were
922 generated and tested as modules in the *in vivo* data. (b and c) Upregulated genes in comparison to
923 the transcriptomes of carriage negative and carriage positive volunteers were compared between
924 time points. Plots represent log2 TPM arithmetic mean for genes in the core (b) and integrated (c)
925 modules. P = <0.05, (one tail Mann-Whitney test). Number of samples for carriage negative and
926 positive, respectively: pre (17:14), day 2 (15:14), day 9 (7:7).

927

928 **Figure 8. Model of pneumococcal colonisation at the human mucosal epithelium.**

929 Pneumococcal adhesion and micro-colony formation on the epithelial surface may lead to micro-
930 invasion; internalisation of the bacteria and/ or transmigration across the epithelial barrier (micro-
931 invasion). The epithelial-derived response is dependent on the subsequent pattern of interactions.
932 Micro-invasion amplifies epithelial sensing and inflammation/ innate immunity, which we postulate
933 leads to immune cell engagement. This process of epithelial sensing inflammation/ innate immunity
934 may enhance both clearance and transmission. Co-association with junctional proteins may facilitate
935 migration across the barrier.

936

Table 1

				Sample day			Pneumococcal association		
ID	Pneumococcal density	Pre	D2	D6	D9	D27	Surface	Intracellular	Lateral
1	Culture (CFU/ml)	0	373	520	10	2			
	Microscopy (counts)	0	+	+	0	+	+	0	0
	LytA PCR	NEG	POS	POS	n/a	POS			
2	Culture (CFU/ml)	0	0	0	0	0			
	Microscopy (counts)	+	+	0	0	0	++	+	0
	LytA PCR	NEG	NEG	NEG	n/a	NEG			
3	Culture (CFU/ml)	0	0	0	0	0			
	Microscopy (counts)	0	+	0	0	0	+	0	0
	LytA PCR	NEG	POS	NEG	n/a	NEG			
4	Culture (CFU/ml)	0	3	9	0	0			
	Microscopy (counts)	0	0	0	+	0	+	0	0
	LytA PCR	NEG	POS	POS	n/a	NEG			
5	Culture (CFU/ml)	0	$7x10^3$	223	22	0			
	Microscopy (counts)	0	+	+	+	0	+	+	0
	LytA PCR	n/a	n/a	n/a	n/a	n/a			
6	Culture (CFU/ml)	0	$1.9x10^4$	$5.7x10^3$	$3.7x10^4$	11			
	Microscopy (counts)	0	++	++++	++	0	+++	++	+
	LytA PCR	NEG	POS	POS	n/a	POS			
7	Culture (CFU/ml)	0	822	$1.1x10^3$	160	0			
	Microscopy (counts)	0	+	+++	++	0	++	+	+
	LytA PCR	NEG	POS	POS	n/a	NEG			
8	Culture (CFU/ml)	0	0	0	0	0			
	Microscopy (counts)	0	0	0	0	0	0	0	0
	LytA PCR	n/a	n/a	n/a	n/a	n/a			
9	Culture (CFU/ml)	0	221	695	4	<1			
	Microscopy (counts)	n/a	+	+++	+	n/a	+++	+	+
	LytA PCR	NEG	POS	POS	n/a	NEG			
10	Culture (CFU/ml)	0	$1x10^3$	0	0	0			
	Microscopy (counts)	n/a	0	+	0	n/a	+	0	0
	LytA PCR	NEG	POS	POS	n/a	POS			
11	Culture (CFU/ml)	0	$1.8x10^6$	$1.8x10^6$	$1.9x10^4$	<1			
	Microscopy (counts)	n/a	++++	++++	+	n/a	+++	+	+
	LytA PCR	NEG	POS	POS	n/a	NEG			
12	Culture (CFU/ml)	0	0	0	0	0			
	Microscopy (counts)	n/a	++	0	0	n/a	++	+	+
	LytA PCR	NEG	NEG	NEG	n/a	NEG			
13	Culture (CFU/ml)	0	23	2	0	0			
	Microscopy (counts)	n/a	+	0	0	n/a	+	0	0
	LytA PCR	POS	POS	POS	n/a	POS			

Figure 1

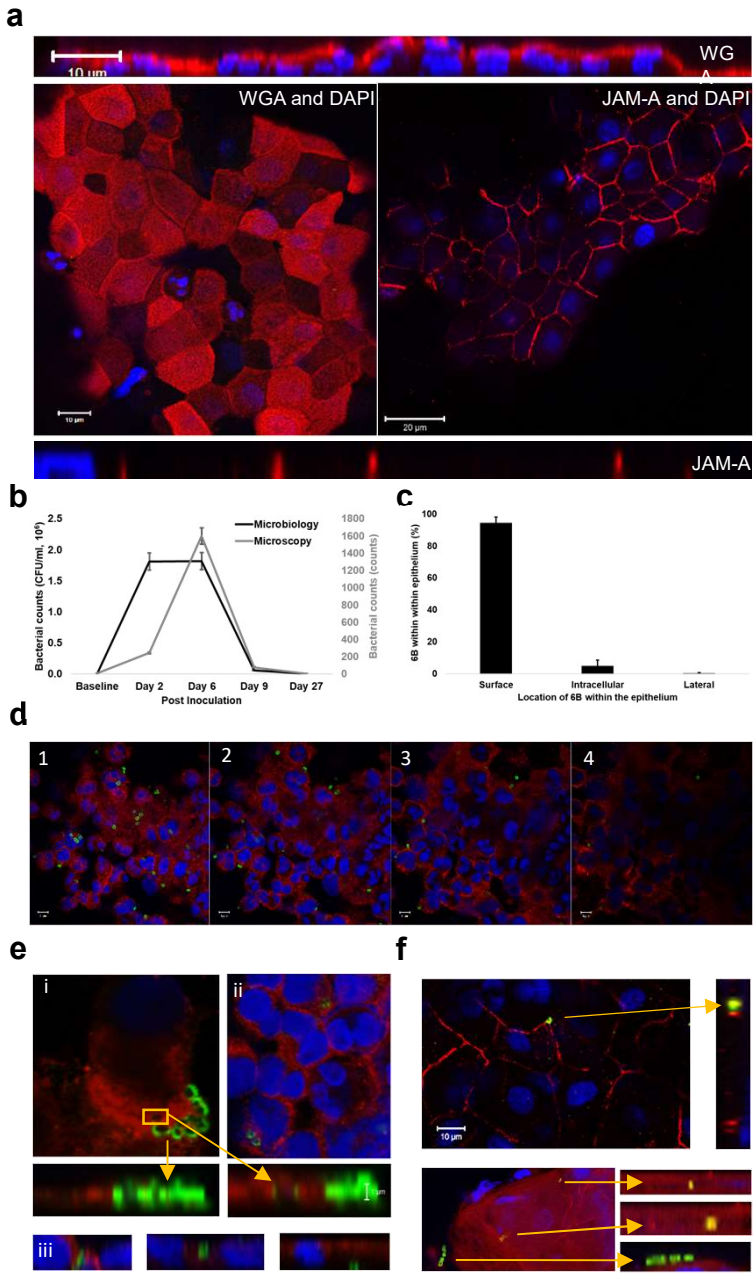
a
10 µm
WGA and DAPI
JAM-A and DAPI
20 µm
JAM-A
b
Microbiology
Microscopy
Bacterial counts (CFU/ml, 10⁶)
Bacterial counts (counts)
Baseline
Day 2
Day 6
Day 9
Day 27
Post Inoculation
c
6B within within epithelium (%)
Surface
Intracellular
Lateral
Location of 6B within the epithelium
d
1
2
3
4
e
i
ii
iii
f
10 µm

Figure 2

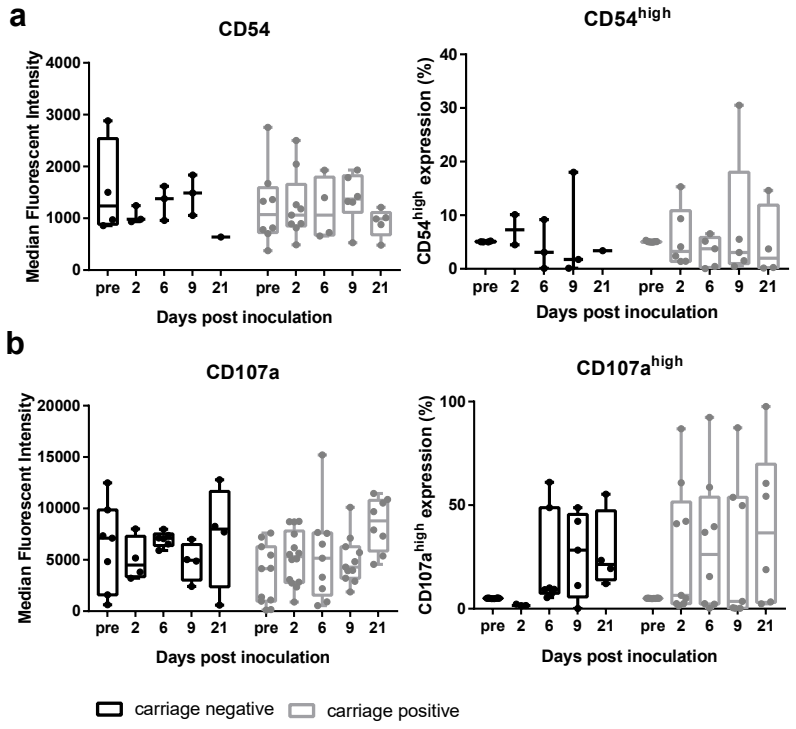
a
CD54
Median Fluorescent Intensity
4000
3000
2000
1000
0
pre 2 6 9 21 pre 2 6 9 21
Days post inoculation
CD54high
CD54high expression (%)
40
30
20
10
0
pre 2 6 9 21 pre 2 6 9 21
Days post inoculation
b
CD107a
Median Fluorescent Intensity
20000
15000
10000
5000
0
pre 2 6 9 21 pre 2 6 9 21
Days post inoculation
CD107ahigh
CD107ahigh expression (%)
100
50
0
pre 2 6 9 21 pre 2 6 9 21
Days post inoculation
carriage negative
carriage positive

Figure 3

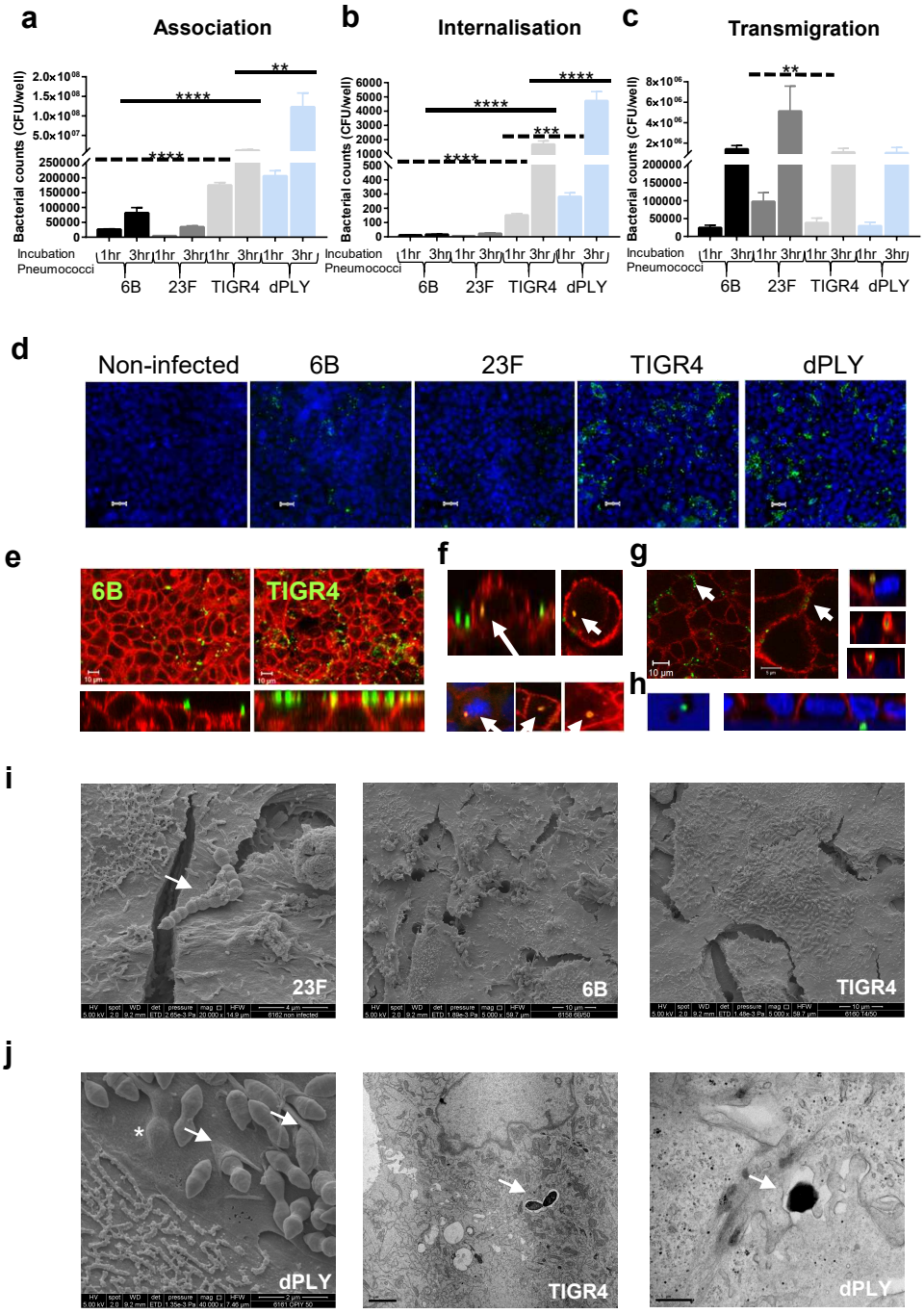
a
Association
b
Internalisation
c
Transmigration
Bacterial counts (CFU/well)
Incubation
Pneumococci
1hr 3hr 1hr 3hr 1hr 3hr 1hr 3hr
6B 23F TIGR4 dPLY
d
Non-infected
6B
23F
TIGR4
dPLY
e
6B
TIGR4
f
g
h
i
23F
6B
TIGR4
j
dPLY
TIGR4
dPLY

Figure 4

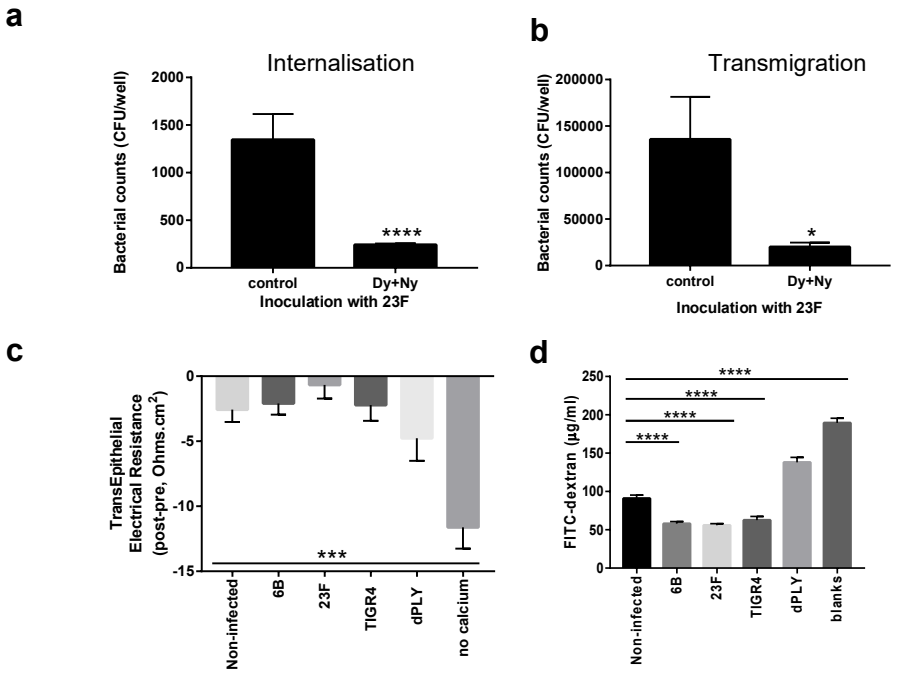
a
Internalisation
Bacterial counts (CFU/well)
2000
1500
1000
500
0
****
control
Dy+Ny
Inoculation with 23F
b
Transmigration
Bacterial counts (CFU/well)
200000
150000
100000
50000
0
*
control
Dy+Ny
Inoculation with 23F
c
TransEpithelial Electrical Resistance (post-pre, Ohms.cm2)
0
-5
-10
-15
***
Non-infected
6B
23F
TIGR4
dPLY
no calcium
d
FITC-dextran (µg/ml)
250
200
150
100
50
0
****
****
****
****
Non-infected
6B
23F
TIGR4
dPLY
blanks

Figure 5

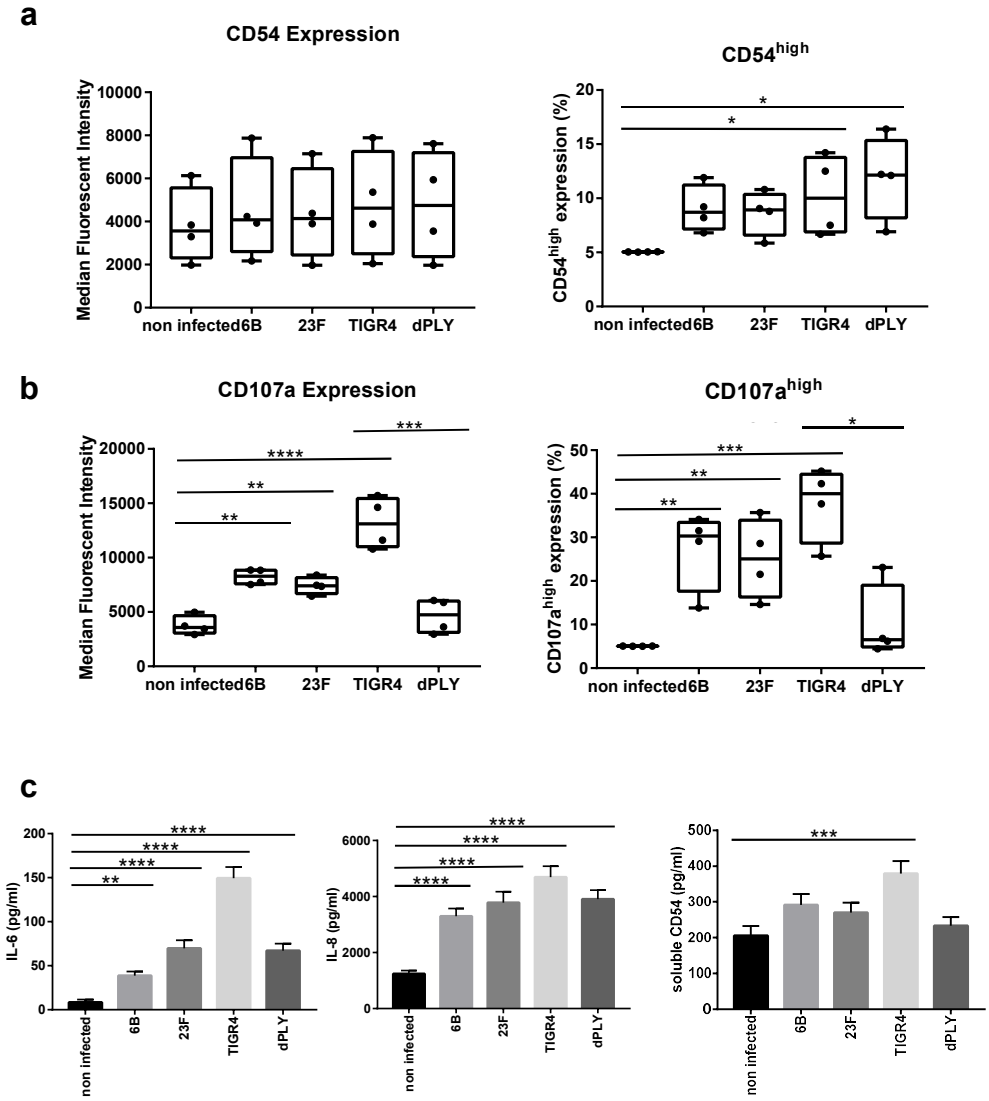
a
CD54 Expression
Median Fluorescent Intensity
10000
8000
6000
4000
2000
0
non infected
6B
23F
TIGR4
dPLY
CD54high
CD54high expression (%)
20
15
10
5
0
*
*
b
CD107a Expression
Median Fluorescent Intensity
20000
15000
10000
5000
0
****
**
**
***
CD107ahigh
CD107ahigh expression (%)
50
40
30
20
10
0
***
**
**
*
c
IL-6 (pg/ml)
200
150
100
50
0
****
****
****
**
IL-8 (pg/ml)
6000
4000
2000
0
****
****
****
****
soluble CD54 (pg/ml)
500
400
300
200
100
0
***
non infected
6B
23F
TIGR4
dPLY

Figure 6

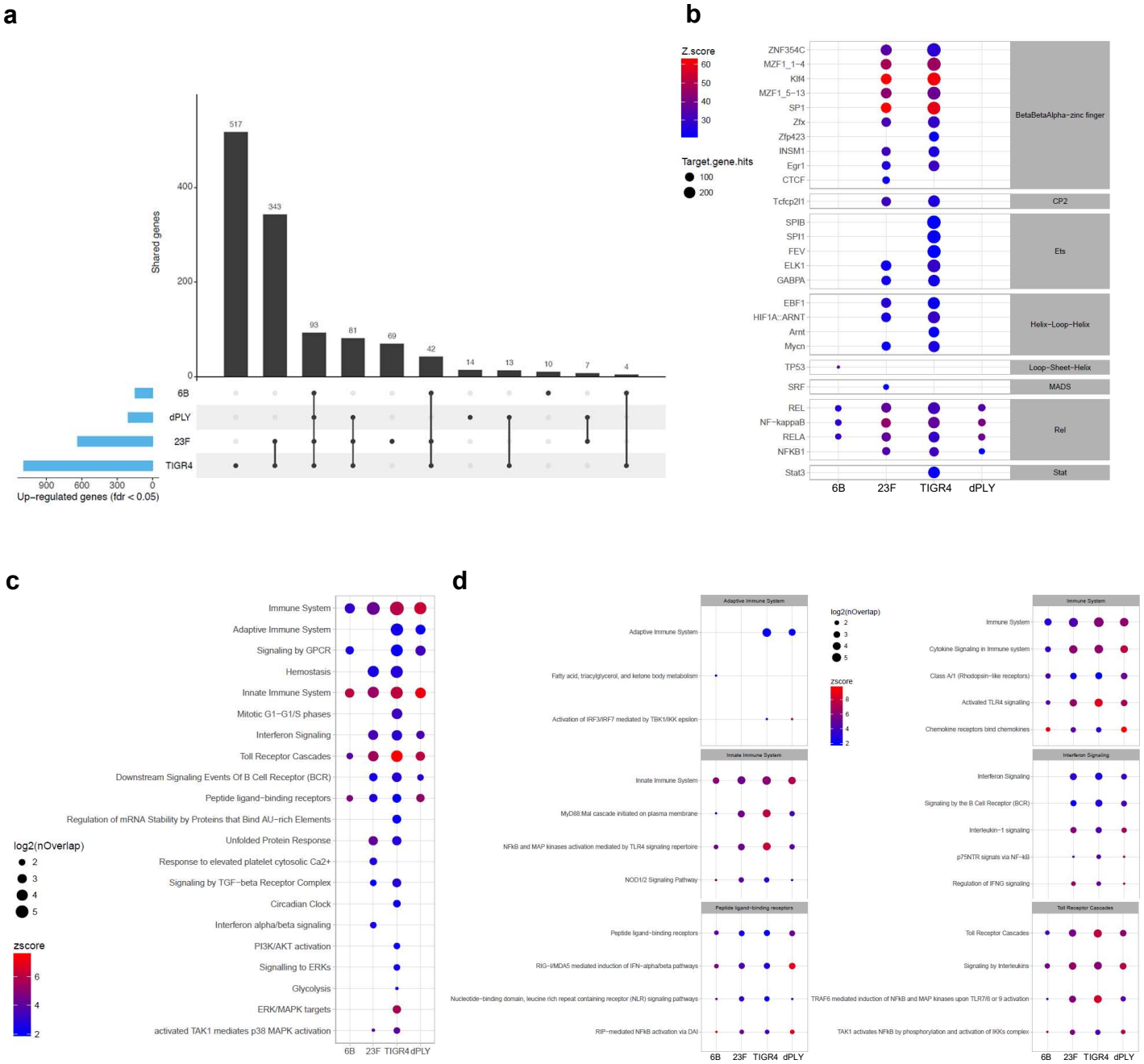
a
Shared genes
517
343
93
81
69
42
14
13
10
7
4
6B
dPLY
23F
TIGR4
Up-regulated genes (fdr < 0.05)
b
Z.score
Target.gene.hits
ZNF354C
MZF1_1-4
Klf4
MZF1_5-13
SP1
Zfx
Zfp423
INSM1
Egr1
CTCF
BetaBetaAlpha-zinc finger
Tcfcp2l1
CP2
SPIB
SPI1
FEV
ELK1
GABPA
Ets
EBF1
HIF1A::ARNT
Arnt
Mycn
Helix-Loop-Helix
TP53
Loop-Sheet-Helix
SRF
MADS
REL
NF-kappaB
RELA
NFKB1
Rel
Stat3
Stat
6B
23F
TIGR4
dPLY
c
Immune System
Adaptive Immune System
Signaling by GPCR
Hemostasis
Innate Immune System
Mitotic G1-G1/S phases
Interferon Signaling
Toll Receptor Cascades
Downstream Signaling Events Of B Cell Receptor (BCR)
Peptide ligand-binding receptors
Regulation of mRNA Stability by Proteins that Bind AU-rich Elements
Unfolded Protein Response
Response to elevated platelet cytosolic Ca2+
Signaling by TGF-beta Receptor Complex
Circadian Clock
Interferon alpha/beta signaling
PI3K/AKT activation
Signalling to ERKs
Glycolysis
ERK/MAPK targets
activated TAK1 mediates p38 MAPK activation
log2(nOverlap)
zscore
6B
23F
TIGR4
dPLY
d
Adaptive Immune System
Fatty acid, triacylglycerol, and ketone body metabolism
Activation of IRF3/IRF7 mediated by TBK1/IKK epsilon
Innate Immune System
MyD88:Mal cascade initiated on plasma membrane
NFkB and MAP kinases activation mediated by TLR4 signaling repertoire
NOD1/2 Signaling Pathway
Peptide ligand-binding receptors
RIG-I/MDA5 mediated induction of IFN-alpha/beta pathways
Nucleotide-binding domain, leucine rich repeat containing receptor (NLR) signaling pathways
RIP-mediated NFkB activation via DAI
Immune System
Cytokine Signaling in Immune system
Class A/1 (Rhodopsin-like receptors)
Activated TLR4 signalling
Chemokine receptors bind chemokines
Interferon Signaling
Signaling by the B Cell Receptor (BCR)
Interleukin-1 signaling
p75NTR signals via NF-kB
Regulation of IFNG signaling
Toll Receptor Cascades
Signaling by Interleukins
TRAF6 mediated induction of NFkB and MAP kinases upon TLR7/8 or 9 activation
TAK1 activates NFkB by phosphorylation and activation of IKKs complex
log2(nOverlap)
zscore
6B
23F
TIGR4
dPLY

Figure 7

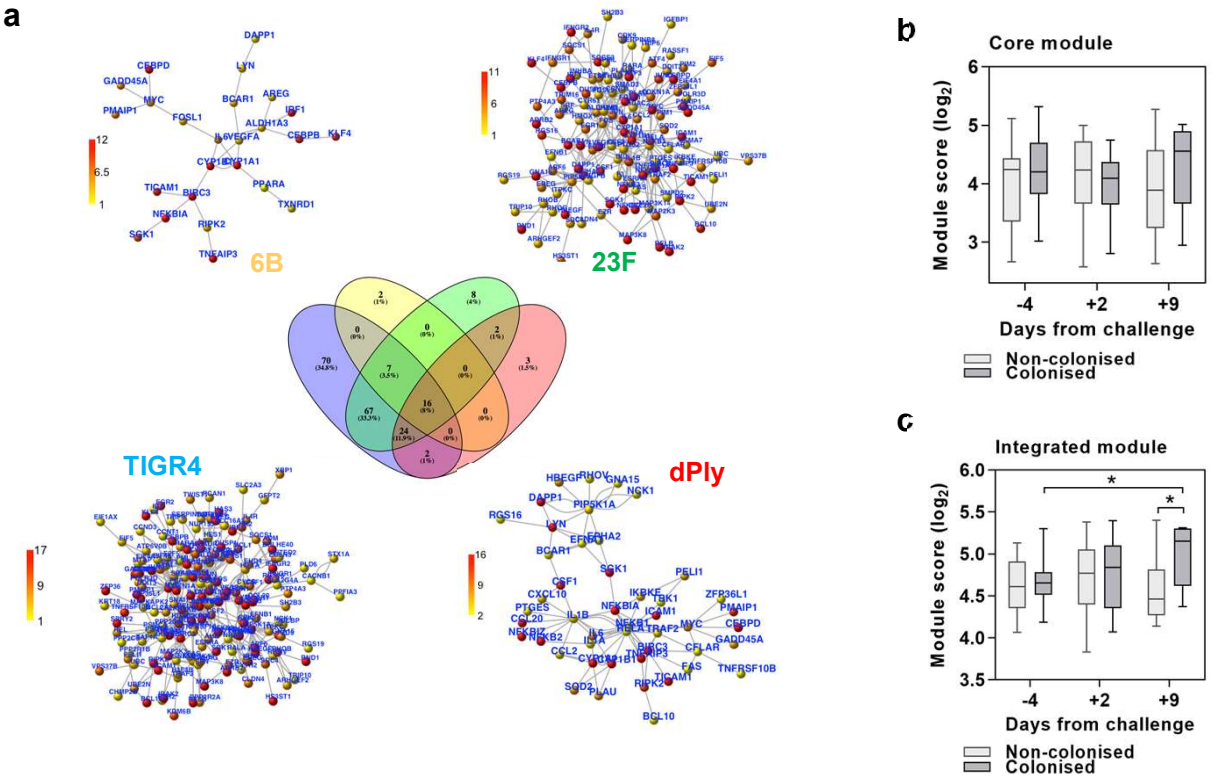
a
6B
23F
TIGR4
dPly
b
Core module
Module score (log2)
Days from challenge
-4
+2
+9
Non-colonised
Colonised
c
Integrated module
Module score (log2)
Days from challenge
-4
+2
+9
Non-colonised
Colonised

Figure 8

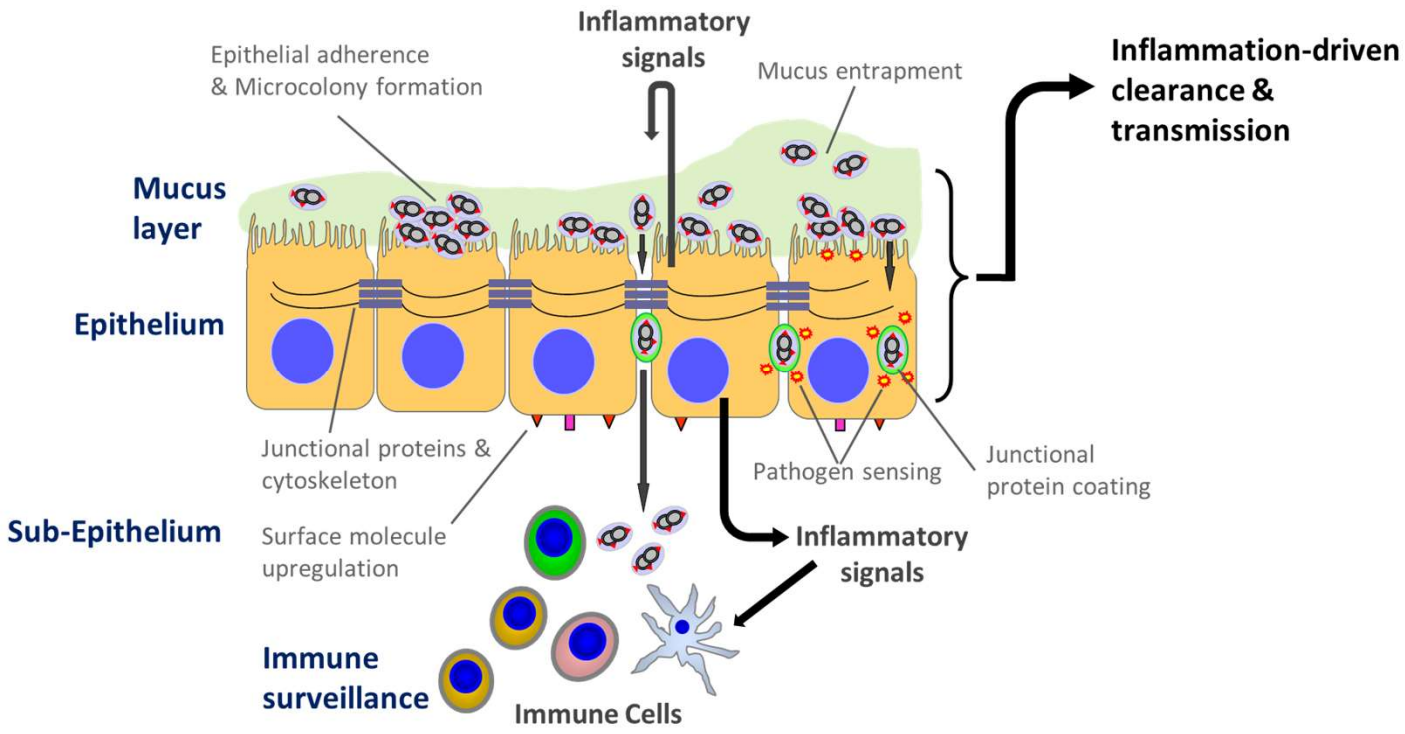
Inflammatory signals
Epithelial adherence & Microcolony formation
Mucus entrapment
Inflammation-driven clearance & transmission
Mucus layer
Epithelium
Junctional proteins & cytoskeleton
Pathogen sensing
Junctional protein coating
Sub-Epithelium
Surface molecule upregulation
Inflammatory signals
Immune surveillance
Immune Cells